Physiol Genomics 40: 94–99, 2010.
First published October 27, 2009; doi:10.1152/physiolgenomics.00123.2009.

Identification and characterization of a novel *ABCA3* mutation

Sang-Kyu Park,[1,2,3]* Louella Amos,[1]* Aparna Rao,[1] Michael W. Quasney,[1,2,3] Yoshihiro Matsumura,[4] Nobuya Inagaki,[5] and Mary K. Dahmer[1,2,3]

[1]*Department of Pediatrics,* [2]*Children's Research Institute, and* [3]*Human and Molecular Genetics Center, Medical College of Wisconsin, Milwaukee, Wisconsin;* [4]*Department of Biochemistry and Molecular Biology, Oregon Health and Science University, Portland, Oregon; and* [5]*Department of Diabetes and Clinical Nutrition, Kyoto University, Kyoto, Japan*

Submitted 31 July 2009; accepted in final form 25 October 2009

Park SK, Amos L, Rao A, Quasney MW, Matsumura Y, Inagaki N, Dahmer MK. Identification and characterization of a novel *ABCA3* mutation. *Physiol Genomics* 40: 94–99, 2010. First published October 27, 2009; doi:10.1152/physiolgenomics.00123.2009.—Mutations in the gene coding for ATP-binding cassette protein A3 (ABCA3) are recognized as a genetic cause of lung disease of varying severity. Characterization of a number of mutant ABCA3 proteins has demonstrated that the mutations generally affect intracellular localization or the ability of the protein to hydrolyze ATP. A novel heterozygous mutation that results in the substitution of cysteine for arginine at amino acid 295 in ABCA3 was identified in a premature infant with chronic respiratory insufficiency and abnormal lamellar bodies. Sequencing of DNA performed in study participants demonstrated that this was a mutation and not a common variant. Plasmid vectors containing *ABCA3* with the identified novel mutation tagged with green fluorescent protein on the carboxy terminus were generated. The effect of the mutation on protein function was characterized by examining the glycosylation state of the mutant protein in transiently transfected HEK293 cells and by examining ATP hydrolysis activity of the mutant protein with a vanadate-induced nucleotide trapping assay in stably transfected HEK293 cells. The ABCA3 protein containing the R295C mutation undergoes normal glycosylation and intracellular localization but has dramatically reduced ATP hydrolysis activity (12% of wild type). The identification of one copy of this novel mutation in a premature infant with chronic respiratory insufficiency suggests that *ABCA3* haploinsufficiency together with lung prematurity may result in more severe, or more prolonged, respiratory failure.

chronic respiratory insufficiency; surfactant; pediatrics; lung disease

SURFACTANT IS ESSENTIAL for normal lung function partly by lowering alveolar surface tension and preventing end-expiratory atelectasis. Surfactant is found in lamellar bodies in type II pneumocytes and is composed of phospholipids and the surfactant-associated proteins SP-A, SP-B, SP-C, and SP-D. Inherited mutations in SP-B and SP-C are associated with respiratory failure (6, 10, 18). Loss-of-function mutations on both alleles of SP-B result in surfactant deficiency, severe neonatal lung disease, and in some instances death. SP-C deficiency is generally less severe, resulting in a spectrum of respiratory problems, ranging from neonatal disease to childhood interstitial lung disease.

Recently, mutations in the ATP-binding cassette protein A3 (ABCA3) gene have been recognized as another cause of surfactant deficiency and lung disease (1, 2, 10, 20). ABCA3 is a member of the ABC family of transmembrane proteins involved in the transport of a variety of substrates across membranes (11). ABC proteins bind and hydrolyze ATP, and hydrolysis of ATP is required for the protein to function as a transporter. ABCA3 is specifically found in the limiting membrane of surfactant-storing intracellular lamellar bodies in type II alveolar epithelial cells (16, 21). Recent evidence indicates that ABCA3 transports lipids essential for surfactant synthesis and function into lamellar bodies (5, 8, 15, 17).

Mutations in *ABCA3* have been found to cause lung disease of varying severity. Over 70 *ABCA3* mutations have been identified in full-term infants with respiratory failure and children with interstitial lung disease (10), although the functional impact of many of these mutants has not been explored. Little is known about the effect of *ABCA3* mutations on premature infants who are predisposed to chronic lung disease because of their prematurity, although there is one report suggesting that a single nucleotide polymorphism (SNP) in *ABCA3* may be associated with a prolonged course of respiratory distress syndrome (RDS) in very premature infants (12).

In the present study, we have identified a novel mutation in the gene coding for ABCA3 in a premature Hmong infant with chronic respiratory insufficiency. This mutation substitutes a cysteine for an arginine at amino acid position 295 in the first intracellular loop (ICL-1) of ABCA3. Functional analysis of this R295C mutation demonstrates that the mutation severely compromises the ability of the protein to hydrolyze ATP.

MATERIALS AND METHODS

Enrollment of subjects. Individuals of a Hmong community in Wisconsin eligible for enrollment included *1*) healthy unrelated adults ≥18 yr of age of Hmong descent on no medications or *2*) parents and relatives of the index case. Subjects were identified through community outreach and the parents of the index case. Subjects who could not speak English were excluded, as were individuals whose immediate family member or first-degree relative was already enrolled. Research personnel obtained written consent from eligible subjects, and a buccal swab was obtained. A unique code was applied to the swab, and no identifiers were obtained by the investigators, with the exception of the parents and relatives of the index case. This study was approved by the Institutional Review Board.

DNA analysis. Buccal swabs were stored at −20°C until extraction. DNA was extracted from buccal swabs with the Epicentre MasterAmp Buccal Swab DNA Extraction kit (MB79015) and stored at −80°C.

DNA samples were amplified in the region of the variant with AmpliTaq Gold polymerase (Applied Biosystems, Foster City, CA) and the primers 5′-TCACCTTGACACAGAAGAGCAG-3′ and 5′-AGTAAGACCCTGTCGAATGCAG-3′. The PCR reaction conditions were 96°C for 5 min followed by 40 cycles of 94°C for 30 s, 55°C for 30 s, 72°C for 45 s, followed by 72°C for 10 min. The PCR product (248 bp) was treated with ExoSAP-IT (USB, Cleveland, OH) and sequenced.

* S.-K. Park and L. Amos contributed equally to the project and authorship of the manuscript.

Address for reprint requests and other correspondence: M. K. Dahmer, Div. of Critical Care, Dept. of Pediatrics, Medical College of Wisconsin, 9000 West Wisconsin Ave., MS681, Milwaukee, WI 53201 (e-mail: mdahmer@mcw.edu).

Cell culture. HEK293 cells purchased from American Type Culture Collection (Manassas, VA) were maintained in Dulbecco's modified Eagle's medium (DMEM; Invitrogen, Carlsbad, CA) supplemented with penicillin (100 U/ml), streptomycin (100 μg/ml), 25 mM HEPES, and 10% fetal bovine serum (FBS) in a humidified atmosphere of 5% CO_2 at 37°C.

DNA construction. The R295C mutant was initially generated from the pEGFPN1-ABCA3-green fluorescent protein (GFP) construct (14) with the QuikChange II XL site-directed mutagenesis kit (Stratagene, La Jolla, CA) and the following primers: forward 5′-AGGCTGAAGGAGTACATGTGCATGATGGGGCTCAGCAG-3′ and reverse 5′-CTGCTGAGCCCCATCATGCACATGTACTCCTTCAGCCT-3′ (underlines indicate substituted nucleotides). A R295C-GFP construct in a pCAGIpuro vector was generated by inserting the coding region of ABCA3-R295C-GFP into the pCAGIpuro vector. Presence of the mutation in the pEGFN1-ABCA3-R295C-GFP and pCAGIpuro-ABCA3-R295C-GFP constructs was confirmed by sequencing.

Glycosylation of wild-type and mutant ABCA3-GFP proteins. Transient transfections of HEK293 cells with wild-type *ABCA3*-GFP and *ABCA3* mutants L101P-GFP, N568D-GFP, and L982P-GFP (14), as well as the new pEGFPN1 construct for R295C-GFP, were performed with FuGENE 6 transfection reagent (Roche Applied Science, Indianapolis, IN) as previously described (14). Briefly, for each experiment cells were seeded into 100-mm dishes at a density of 3×10^6/dish for the assay and cultured for 1 day, and each plate was then transfected with 6 μg of one of the plasmid vectors listed above. Cells were cultured for an additional 48 h and lysed, and membranes were prepared as described previously (14). Membrane protein (10 μg) was treated with 100 U of peptide N-glycosidase F (PNGase F) or 500 U of endoglycosidase H (Endo H) (New England Biolabs, Beverly, MA) for 30 min at 37°C in a total volume of 20 μl. The samples were then electrophoresed on 5% SDS-polyacrylamide gels, and immunoblot analysis was performed with anti-GFP monoclonal antibody (Santa Cruz Biotechnology, Santa Cruz, CA).

Stable transfection of wild-type and mutant ABCA3-GFP. Clonally selected HEK293 cell lines stably expressing wild-type or various mutant *ABCA3*-GFP genes were developed as previously described (14) and maintained in DMEM containing 2.5 μg/ml puromycin (Sigma, St. Louis, MO).

Vanadate-induced nucleotide trapping assay of wild-type and mutant ABCA3-GFP proteins. Vanadate-induced nucleotide trapping was performed with 8-azido-[α-^{32}P]ATP purchased from Affinity Labeling Technologies (ALT, Lexington, KY) as described previously (14). Samples were analyzed by SDS-PAGE on 5% polyacrylamide gel, electrotransferred onto nitrocellulose membranes (Bio-Rad, Hercules, CA), and quantified with a STORM 860 PhosphorImager system (Amersham Biosciences, Piscataway, NJ). Each experiment was performed on a different passage of stably transfected cell lines.

RESULTS

Identification of a novel R295C mutation. A Hmong male born at 25 wk of gestation (weighing 790 g) was intubated at birth and received surfactant therapy for RDS. He required high-frequency oscillatory ventilation for 2½ mo and conventional mechanical ventilation for 1 mo and was eventually transitioned to noninvasive ventilation. After a 4-mo hospitalization in the neonatal intensive care unit, he was discharged on oxygen therapy with a nasal cannula. Within 4 wk of discharge, he was hospitalized with worsening respiratory failure, increasing oxygen need, and poor weight gain. Chest computerized tomography demonstrated coarse interstitial opacities, cystic changes, and focal hyperinflation, while bronchoscopy revealed normal upper and lower airway anatomy. Despite appropriate medical therapies, the child was hospital-

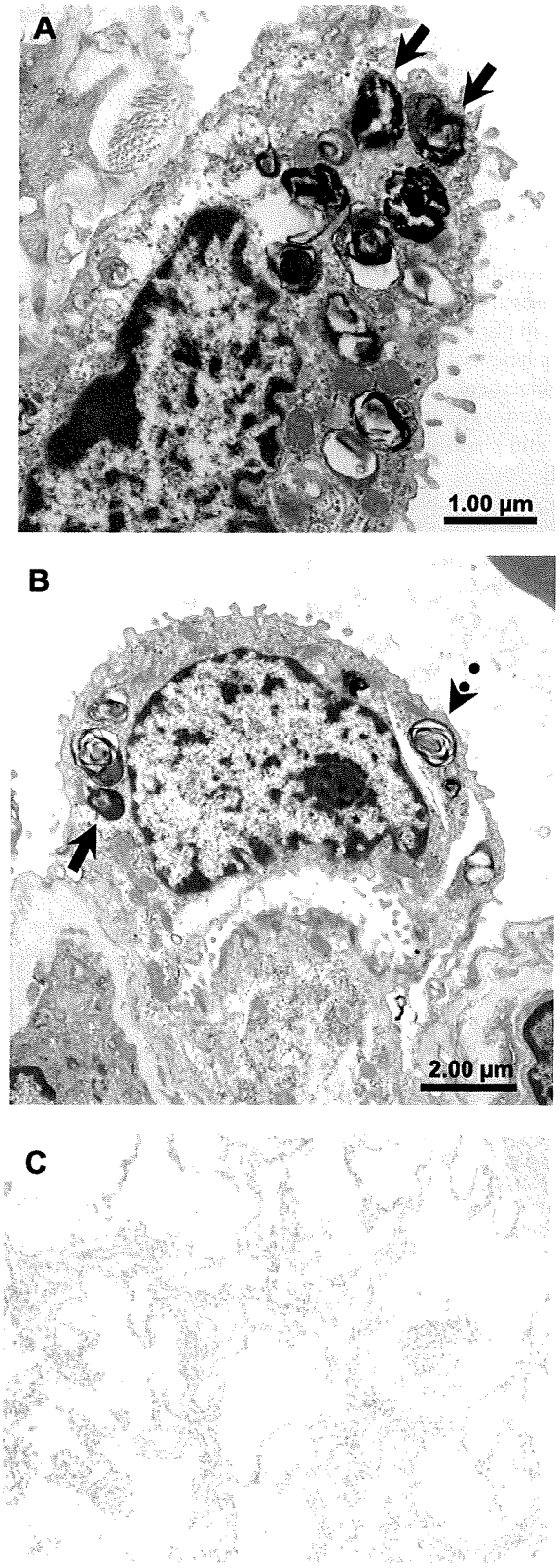

Fig. 1. Microscopy of the lung biopsy from a patient with chronic respiratory insufficiency. *A* and *B*: electron microscopy demonstrating abnormal lamellar bodies (solid arrows) and normal lamellar bodies (dashed arrows). Some cells have a combination of normal and abnormal lamellar bodies. *C*: hematoxylin and eosin staining (magnification ×20) demonstrating irregular dilatation and reduced number of peripheral alveoli with thickened smooth muscle in arterial walls.

ized during the majority of his first year of life for refractory respiratory insufficiency and eventually had a tracheostomy at age 1 yr. To determine whether the chronic respiratory insufficiency observed might be due to an inherited disorder resulting in surfactant deficiency, genetic testing (for mutations in the genes for SP-B, SP-C, and ABCA3 by sequencing of exons and splice sites) and a lung biopsy were performed. Lung biopsy demonstrated the presence of abnormal lamellar bodies (Fig. 1; some normal lamellar bodies were also observed) and chronic bronchopulmonary dysplasia (BPD) with persistent fetal pulmonary architecture. DNA sequencing revealed no mutations in the genes coding for SP-B and SP-C; however, the child was heterozygous for a novel variation in the *ABCA3* gene (replacement of a C with a T at nucleotide position 883). This change results in the replacement of arginine by cysteine at amino acid position 295. No other mutations in *ABCA3* were identified.

Although the R295C variant had not been observed in previously characterized populations, it was unclear whether the R295C variant was a common polymorphism in Hmong individuals or a clinically significant mutation. To determine whether the R295C variant was a polymorphism or a mutation, the frequency of this variant in the Hmong population was examined. DNA from individuals from the child's family, and from individuals in the Hmong community, was sequenced in the region of the variation. DNA samples from 90 of 91 individuals from the general Hmong population were sequenced successfully. None of these individuals had the R295C variant, indicating that this variation is indeed a mutation and not a polymorphism. Several members of the child's immediate family, including one of the parents, were heterozygous for the mutation.

Effects of ABCA3 R295C mutation on function. The R295C mutation is located in the first ICL (ICL-1) of the protein (Fig. 2*A*) and is adjacent to the previously reported mutant E292V (2). The R295C mutation resides in a region that is conserved in different members of the ABCA subfamily (Fig. 2*B*) and across ABCA3 homologs in vertebrates (Fig. 2*C*). Previous studies (4, 13, 14) have identified mutations that affect ABCA3 function by either altering intracellular localization (type I mutants) or impairing ATP hydrolysis activity (type II mutants).

To examine whether the intracellular localization of the R295C mutant was altered, the glycosylation state of the R295C mutant was characterized. Membranes from HEK293 cells expressing wild-type *ABCA3*-GFP, the R295C-GFP mutant, or several previously characterized mutants were examined for sensitivity to the glycosidases Endo H and PNGase F. In HEK293 cells, wild-type ABCA3-GFP is mainly localized in lysosomal organelles, mimicking the trafficking of ABCA3 to lamellar bodies in alveolar type II cells (14). Because Endo H only cleaves sugars from high-mannose oligosaccharides, and not from complex oligosaccharides, resistance to Endo H indicates that the protein is in post-Golgi membranes (presumably lamellar body-like organelles). After treatment

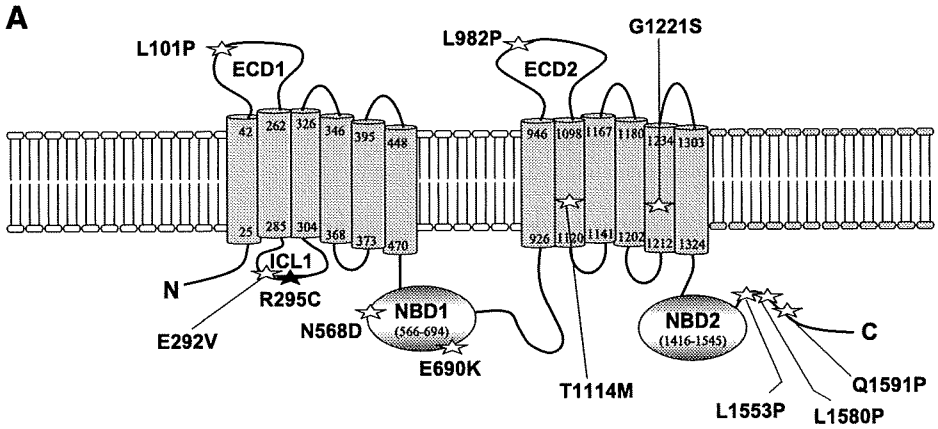

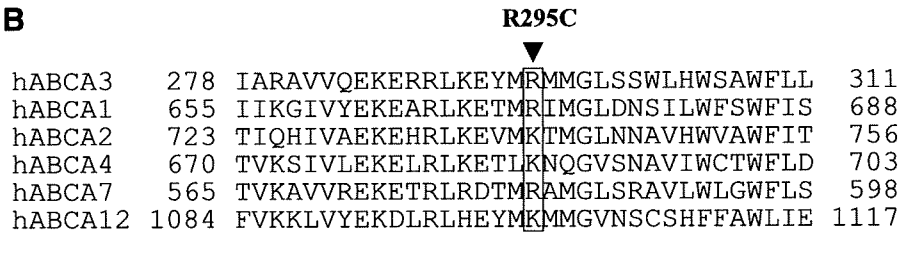

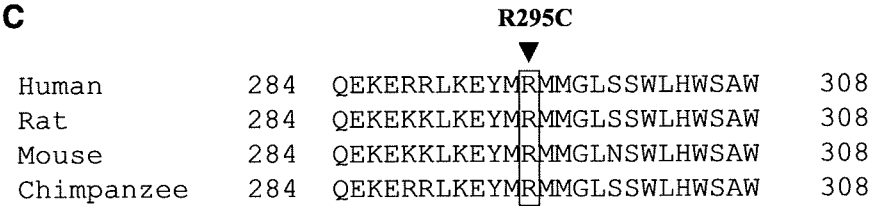

Fig. 2. Schematic diagram of ATP-binding cassette protein A3 (ABCA3) and conservation of amino acids in the region of the R295C mutant. *A*: schematic diagram of the ABCA3 protein. ☆, Mutations reported previously; ★, novel mutant R295C. ECD1 and ECD2, extracellular domains; ICL-1, intracellular loop 1; NBD1 and NBD2, nucleotide binding domains. Type I mutations include L101P, L982P, L1553P, and Q1591P; type II mutations include E292V, N568D, E690K, T1114, G1221S, and L1580P (13, 14). *B*: alignment of sequences surrounding the R295C mutation in ICL-1 in various members of the ABCA subfamily. *C*: alignment of sequences surrounding the R295C mutation in human, rat, mouse, and chimpanzee.

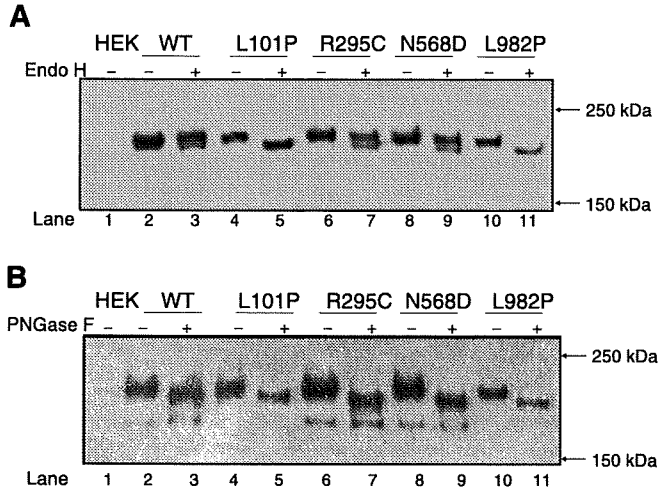

Fig. 3. Glycosylation of wild-type (WT) and mutant ABCA3-green fluorescent protein (GFP) proteins. *A*: 20 μg of membrane fraction from HEK293 cells transiently transfected with WT ABCA3-GFP (*lanes 2* and *3*) or with ABCA3-GFP mutants L101P (*lanes 4* and *5*), R295C (*lanes 6* and *7*), N568D (*lanes 8* and *9*), and L982P (*lanes 10* and *11*) were treated without (−) or with (+) endoglycosidase H (Endo H) and analyzed by 5% SDS-PAGE followed by immunoblotting with anti-GFP antibody. *Lane 1*, immunoblotting of untransfected HEK293 cells. *B*: WT ABCA3-GFP (*lanes 2* and *3*) or ABCA3-GFP mutants L101P (*lanes 4* and *5*), R295C (*lanes 6* and *7*), N568D (*lanes 8* and *9*), and L982P (*lanes 10* and *11*) were treated without (−) or with (+) peptide N-glycosidase F (PNGase F) and were then analyzed by 5% SDS-PAGE followed by immunoblotting with anti-GFP antibody. *Lane 1*, immunoblotting of untransfected HEK293 cells. Results from 1 representative experiment from a total of 3 separate experiments are shown.

with Endo H the wild-type ABCA3 protein is present as a doublet (Fig. 3*A*, *lane 3*), with much of the protein being resistant to Endo H, suggesting it is in post-Golgi membranes (Fig. 3*A*, compare *lanes 2* and *3*). This observation is consistent with previous reports. The R295C variant demonstrated a level of resistance to Endo H comparable to that of the wild-type protein (Fig. 3*A*, compare *lanes 6* and *7* to *lanes 2* and *3*), suggesting that the variant protein has undergone normal glycosylation and resides in post-Golgi membranes. As reported previously, the N568D variant shows resistance to Endo H (Fig. 3*A*, *lanes 8* and *9*) at a level similar to that of the wild-type protein; however, the L101P and L982P variants (Fig. 3*A*, *lanes 4* and *5* and *lanes 10* and *11*, respectively) show no Endo H resistance, indicating that these mutants have not left the endoplasmic reticulum (14). As expected, the wild-type and mutant ABCA3 proteins are all sensitive to PNGase F (Fig. 3*B*), which cleaves both high-mannose and complex oligosaccharide from N-linked glycoproteins.

To determine whether the R295C mutation affected the ATP hydrolysis activity of the R295C mutant, vanadate-induced nucleotide trapping with photoaffinity labeling of the trapped intermediate (3) was examined. In this assay, ATP hydrolysis with production of a stable intermediate can be assessed based on the intensity of photoaffinity labeling of the ABCA3 protein. As shown in Fig. 4*A*, the level of vanadate-induced nucleotide trapping in the R295C mutant was greatly reduced compared with that of the wild-type ABCA3 protein. The level of the ABCA3-R295C-GFP mutant protein was comparable to that of wild-type ABCA3-GFP as demonstrated in the anti-GFP immunoblot. Vanadate-induced nucleotide trapping was also decreased in the N568D mutant as reported previously (14). Quantitation of three independent experiments demonstrated that the degree of trapping in the R295C mutant was dramatically reduced to 12% of that of the wild type (Fig. 4*B*). These results indicate that the ability of the R295C mutant to hydrolyze ATP is severely impaired.

DISCUSSION

The results presented here demonstrate that R295C is a novel mutation that results in severely impaired ATP hydrolysis activity as indicated by the dramatic reduction in vanadate-induced nucleotide trapping. Other mutations in the ABCA3 protein also result in impaired ATP hydrolysis, including E292V, N568D, G1221S, L1580P, and T1114M (13, 14). The E292V mutation is in ICL-1 only three amino acids from the R295C mutation. Clearly, the presence of two mutations that affect ATP hydrolysis in this ICL suggests that the ICL is important for normal ATP hydrolysis activity and normal

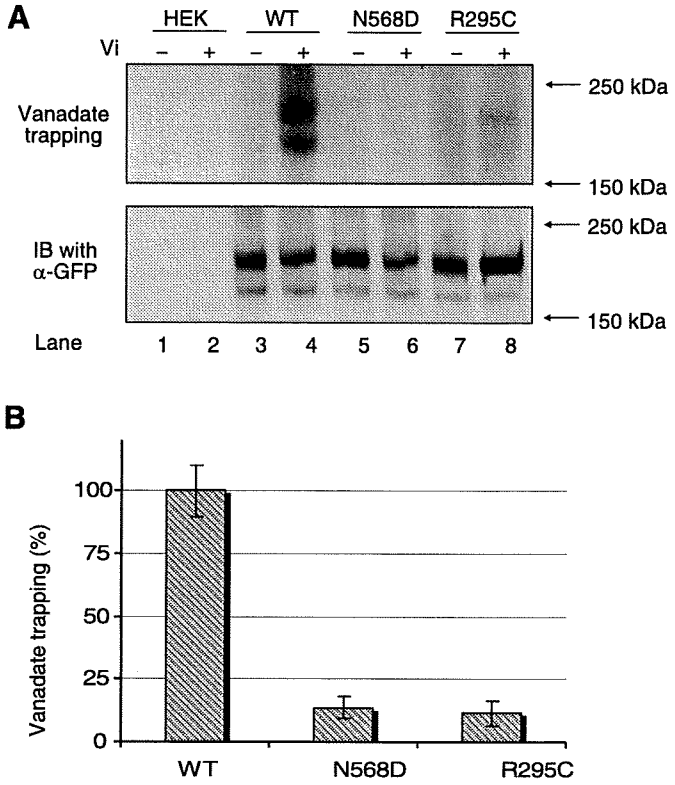

Fig. 4. Vanadate-induced nucleotide trapping in ABCA3-GFP and ABCA3-GFP mutants. *A*: 20 μg of membrane fraction from untransfected HEK293 cells (*lanes 1* and *2*), HEK293 cells stably expressing WT ABCA3-GFP (*lanes 3* and *4*), ABCA3-GFP mutants N568D (*lanes 5* and *6*), and R295C (*lanes 7* and *8*) were incubated with 20 μM 8-azido-[α-^{32}P]ATP in the absence (−) or presence (+) of 0.4 mM orthovanadate (Vi) and 3 mM $MgCl_2$ as described under MATERIALS AND METHODS. Photoaffinity-labeled ATP was detected by autoradiography (*top*) and immunoblotting (IB) using anti-GFP antibody (α-GFP) was used as a loading control (*bottom*). Results from 1 representative experiment from 3 separate experiments performed are shown. *B*: radioactivity of photoaffinity-labeled protein bands was measured and quantified (220 kDa of upper band intensities + 220 kDa of lower band intensities) with STORM 860 PhosphorImager. These were normalized to ABCA3-GFP protein from immunoblot (220 kDa of upper band intensities + 220 kDa of lower band intensities), and then radioactivity in the absence of orthovanadate was subtracted from that in the presence of orthovanadate. Data shown are means ± SD for 3 separate experiments (n = 3), 1 of which is shown in *A*.

functioning of the protein. This conclusion is also supported by the crystal structure of the bacterial ABC protein SAV1866, which suggests that ICLs transmit conformational changes important for function of the protein (7), and by the report of a mutation that reduces ATP hydrolysis activity in an ICL of multidrug resistance protein 1, another human ABC transporter protein (19).

The R295C mutation does not affect glycosylation and intracellular localization of the protein. The trafficking of proteins accompanies the processing of oligosaccharides from high-mannose to complex sugar types, with the presence of complex oligosaccharides indicating that the protein is in post-Golgi membranes. Resistance to Endo H has been demonstrated previously to be associated with localization of the ABCA3 protein to lamellar body-like organelles (14). Normal glycosylation and intracellular localization of the R295C mutant is indicated by the similar levels of sensitivity to Endo H and PNGase F observed for the wild-type ABCA3-GFP protein and the R295C mutant. The observation that a substantial portion of the R295C mutant protein is resistant to Endo H indicates that the mutation does not affect intracellular localization.

Although it is clear that the mutation impairs the function of the ABCA3 protein, the patient in whom this mutation was discovered is heterozygous for the mutation. While it is possible that either a mutation in a regulatory region of the noncoding sequence or an insertion or deletion of one or more exons might be present in the second copy of the *ABCA3* gene, it is more likely that the child has one normal copy of the *ABCA3* gene and consequently has normal as well as impaired ABCA3 protein. That the mutation has an effect on the cellular level of functional ABCA3 is indicated by the abnormal lamellar bodies observed in the patient's alveolar epithelial cells, although normal lamellar bodies are also present. Because one of the child's parents and two siblings also have the mutation and none has a history of severe lung disease, it is likely that there is sufficient functional ABCA3 present for normal lung function under normal conditions. However, the patient was born prematurely and was exposed to a number of stresses that are not seen in term infants, consequently haploinsufficiency (having just 1 functional copy of the gene) may explain the more severe injury and/or prolonged recovery period observed in this patient. Most premature infants require only supplemental oxygen on discharge from the neonatal intensive care unit; rarely do they need tracheostomy for long-term mechanical ventilation as was required for this patient. (By 2.5 yr old this patient had improved enough that a tracheostomy was no longer required.) This patient's haploinsufficiency may have caused surfactant dysfunction milder than would be expected in an individual homozygous for the mutation, but significant enough to cause chronic respiratory insufficiency in a premature infant. One possibility is that an interaction between the R295C mutation and the patient's prematurity resulted in the severe BPD observed. As has been suggested for individuals heterozygous for functional SP-B mutations (10), it is possible that for children heterozygous for a functional *ABCA3* mutation any environmental or developmental stress that alters *ABCA3* expression may result in more severe respiratory stress because of their already reduced level of functional ABCA3. Interestingly, the frequency of individuals heterozygous for the E292V mutation is elevated in a cohort of children with RDS, suggesting that a mutation in this region might impart increased genetic risk for respiratory insufficiency, even in heterozygotes (9).

In conclusion, clinical management of a premature infant with severe BPD and chronic respiratory failure led to the discovery of the novel *ABCA3* mutation R295C. This mutation, present in ICL-1, does not affect intracellular localization but severely impairs ATP hydrolysis activity of the ABCA3 mutant protein and is likely responsible for the aberrant lamellar bodies observed on lung biopsy. The identification of one copy of this novel mutation in a premature infant with chronic respiratory insufficiency suggests that *ABCA3* haploinsufficiency together with lung prematurity may result in more severe, or more prolonged, respiratory failure. Testing for *ABCA3* mutations in infants with refractory respiratory insufficiency or respiratory failure and a history of prematurity may help identify new mutations, clarify the function of ABCA3 and its various domains, and explain observed clinical deterioration despite appropriate medical management.

ACKNOWLEDGMENTS

We thank Daniel Merchant for excellent technical assistance and Dr. James F. Southern for providing histological analysis.

GRANTS

This work was supported, in part, by the Children's Research Institute at the Medical College of Wisconsin.

DISCLOSURES

No conflicts of interest are declared by the author(s).

REFERENCES

1. **Brasch F, Schimanski S, Muhlfeld C, Barlage S, Langmann T, Aslanidis C, Boettcher A, Dada A, Schroten H, Mildenberger E, Prueter E, Ballmann M, Ochs M, Johnen G, Griese M, Schmitz G.** Alteration of the pulmonary surfactant system in full-term infants with hereditary ABCA3 deficiency. *Am J Respir Crit Care Med* 174: 571–580, 2006.
2. **Bullard JE, Wert SE, Whitsett JA, Dean M, Nogee LM.** ABCA3 mutations associated with pediatric interstitial lung disease. *Am J Respir Crit Care Med* 172: 1026–1031, 2005.
3. **Carrier I, Julien M, Gros P.** Analysis of catalytic carboxylate mutants E552Q and E1197Q suggests asymmetric ATP hydrolysis by the two nucleotide-binding domains of P-glycoprotein. *Biochemistry* 42: 12875–12885, 2003.
4. **Cheong N, Madesh M, Gonzales LW, Zhao M, Yu K, Ballard PL, Shuman H.** Functional and trafficking defects in ATP binding cassette A3 mutants associated with respiratory distress syndrome. *J Biol Chem* 281: 9791–9800, 2006.
5. **Cheong N, Zhang H, Madesh M, Zhao M, Yu K, Dodia C, Fisher AB, Savani RC, Shuman H.** ABCA3 is critical for lamellar body biogenesis in vivo. *J Biol Chem* 282: 23811–23817, 2007.
6. **Cole FS, Nogee LM, Hamvas A.** Defects in surfactant synthesis: clinical implications. *Pediatr Clin North Am* 53: 911–917, 2006.
7. **Dawson RJ, Locher KP.** Structure of a bacterial multidrug ABC transporter. *Nature* 443: 180–185, 2006.
8. **Garmany TH, Moxley MA, White FV, Dean M, Hull WM, Whitsett JA, Nogee LM, Hamvas A.** Surfactant composition and function in patients with ABCA3 mutations. *Pediatr Res* 59: 801–805, 2006.
9. **Garmany TH, Wambach JA, Heins HB, Watkins-Torry JM, Wegner DJ, Bennet K, An P, Land G, Saugstad OD, Henderson H, Nogee LM, Cole FS, Hamvas A.** Population and disease-based prevalence of the common mutations associated with surfactant deficiency. *Pediatr Res* 63: 645–649, 2008.

10. **Hamvas A, Cole FS, Nogee LM.** Genetic disorders of surfactant proteins. *Neonatology* 91: 311–317, 2007.
11. **Kaminski WE, Piehler A, Wenzel JJ.** ABC A-subfamily transporters: structure, function and disease. *Biochim Biophys Acta* 1762: 510–524, 2006.
12. **Karjalainen MK, Haataja R, Hallman M.** Haplotype analysis of ABCA3: association with respiratory distress in very premature infants. *Ann Med* 40: 56–65, 2008.
13. **Matsumura Y, Ban N, Inagaki N.** Aberrant catalytic cycle and impaired lipid transport into intracellular vesicles in ABCA3 mutants associated with nonfatal pediatric interstitial lung disease. *Am J Physiol Lung Cell Mol Physiol* 295: L698–L707, 2008.
14. **Matsumura Y, Ban N, Ueda K, Inagaki N.** Characterization and classification of ATP-binding cassette transporter ABCA3 mutants in fatal surfactant deficiency. *J Biol Chem* 281: 34503–34514, 2006.
15. **Matsumura Y, Sakai H, Sasaki M, Ban N, Inagaki N.** ABCA3-mediated choline-phospholipids uptake into intracellular vesicles in A549 cells. *FEBS Lett* 581: 3139–3144, 2007.
16. **Mulugeta S, Gray JM, Notarfrancesco KL, Gonzales LW, Koval M, Feinstein SI, Ballard PL, Fisher AB, Shuman H.** Identification of LBM180, a lamellar body limiting membrane protein of alveolar type II cells, as the ABC transporter protein ABCA3. *J Biol Chem* 277: 22147–22155, 2002.
17. **Nagata K, Yamamoto A, Ban N, Tanaka AR, Matsuo M, Kioka N, Inagaki N, Ueda K.** Human ABCA3, a product of a responsible gene for ABCA3 for fatal surfactant deficiency in newborns, exhibits unique ATP hydrolysis activity and generates intracellular multilamellar vesicles. *Biochem Biophys Res Commun* 324: 262–268, 2004.
18. **Nogee LM.** Alterations in SP-B and SP-C expression in neonatal lung disease. *Annu Rev Physiol* 66: 601–623, 2004.
19. **Ren XQ, Furukawa T, Yamamoto M, Aoki S, Kobayashi M, Nakagawa M, Akiyama S.** A functional role of intracellular loops of human multidrug resistance protein 1. *J Biochem (Tokyo)* 140: 313–318, 2006.
20. **Shulenin S, Nogee LM, Annilo T, Wert SE, Whitsett JA, Dean M.** ABCA3 gene mutations in newborns with fatal surfactant deficiency. *N Engl J Med* 350: 1296–1303, 2004.
21. **Yamano G, Funahashi H, Kawanami O, Zhao LX, Ban N, Uchida Y, Morohoshi T, Ogawa J, Shioda S, Inagaki N.** ABCA3 is a lamellar body membrane protein in human lung alveolar type II cells. *FEBS Lett* 508: 221–225, 2001.

Diabetologia
DOI 10.1007/s00125-010-1729-5

ARTICLE

Metformin suppresses hepatic gluconeogenesis and lowers fasting blood glucose levels through reactive nitrogen species in mice

Y. Fujita · M. Hosokawa · S. Fujimoto · E. Mukai · A. Abudukadier · A. Obara · M. Ogura · Y. Nakamura · K. Toyoda · K. Nagashima · Y. Seino · N. Inagaki

Received: 25 January 2010 / Accepted: 24 February 2010

Abstract
Aims/hypothesis Metformin, the major target of which is liver, is commonly used to treat type 2 diabetes. Although metformin activates AMP-activated protein kinase (AMPK) in hepatocytes, the mechanism of activation is still not well known. To investigate AMPK activation by metformin in liver, we examined the role of reactive nitrogen species (RNS) in suppression of hepatic gluconeogenesis.
Methods To determine RNS, we performed fluorescence examination and immunocytochemical staining in mouse hepatocytes. Since metformin is a mild mitochondrial complex I inhibitor, we compared its effects on suppression of gluconeogenesis, AMPK activation and generation of the RNS peroxynitrite ($ONOO^-$) with those of rotenone, a representative complex I inhibitor. To determine whether endogenous nitric oxide production is required for $ONOO^-$ generation and metformin action, we used mice lacking endothelial nitric oxide synthase (eNOS).
Results Metformin and rotenone significantly decreased gluconeogenesis and increased phosphorylation of AMPK in wild-type mouse hepatocytes. However, unlike rotenone, metformin did not increase the AMP/ATP ratio. It did, however, increase $ONOO^-$ generation, whereas rotenone did not. Exposure of eNOS-deficient hepatocytes to metformin did not suppress gluconeogenesis, activate AMPK or increase $ONOO^-$ generation. Furthermore, metformin lowered fasting blood glucose levels in wild-type diabetic mice, but not in eNOS-deficient diabetic mice.
Conclusions/interpretation Activation of AMPK by metformin is dependent on $ONOO^-$. For metformin action in liver, intra-hepatocellular eNOS is required.

Y. Fujita · M. Hosokawa (✉) · S. Fujimoto · E. Mukai · A. Abudukadier · A. Obara · M. Ogura · Y. Nakamura · K. Toyoda · K. Nagashima · Y. Seino · N. Inagaki
Department of Diabetes and Clinical Nutrition, Graduate School of Medicine, Kyoto University, 54 Shogoin, Kawahara-cho, Sakyo-ku, Kyoto 606-8507, Japan
e-mail: hosokawa@metab.kuhp.kyoto-u.ac.jp

E. Mukai
Japan Association for the Advancement of Medical Equipment, Tokyo, Japan

Y. Seino
Kansai Electric Power Hospital, Osaka, Japan

S. Fujimoto · K. Nagashima · N. Inagaki
CREST of Japan Science and Technology Cooperation (JST), Kyoto, Japan

Published online: 29 March 2010

Keywords AMP · AMP-activated protein kinase · Endothelial nitric oxide synthase · Gluconeogenesis · Metformin · Nitric oxide · Peroxynitrite · Reactive nitrogen species

Abbreviations

AMPK	AMP-activated protein kinase
BAEC	Bovine aortic endothelial cells
DCDHF	2,7-Dihydrodichlorofluorescein
eNOS	Endothelial nitric oxide synthase
L-NAME	N^{ω}-Nitro-L-arginine methyl ester
NOS	Nitric oxide synthase
OCT1	Organic cation transporter 1
$ONOO^-$	Peroxynitrite
RNS	Reactive nitrogen species

Introduction

Metformin is one of the most commonly used oral glucose-lowering drugs for type 2 diabetes and is recommended as a first-line drug in recent treatment guidelines of the American Diabetes Association and European Association for the Study of Diabetes [1, 2]. The main target tissue of metformin is liver and its major effect is to decrease hepatic glucose output, which occurs largely due to the suppression of gluconeogenesis, leading to lower fasting blood glucose levels without insulin stimulation and weight gain [3–5]. In addition, metformin has beneficial effects on cardiovascular function and reduces cardiovascular risk in type 2 diabetes [6].

Although metformin has been used clinically for several decades, the mechanisms by which it exerts its glucose-lowering effects are still unclear [7]. Recent studies have demonstrated that therapeutic effects of metformin are mediated by activation of AMP-activated protein kinase (AMPK), leading to a decrease in gluconeogenesis and an increase of fatty acid oxidation in liver and of glucose uptake in skeletal muscle [8–10]. AMPK is a serine/threonine kinase that acts as an energy sensor and is activated in response to reductions of cellular energy levels and to environmental stress, including hypoxia, ischaemia, exercise, ATP depletion and oxidative stress [11, 12]. Although it has been known that AMPK is activated by an increase in the AMP/ATP ratio, the AMPK-activating mechanism also involves other pathways that are dependent on upstream AMPK kinases, including LKB1 kinase and calmodulin-dependent protein kinase kinase in liver and skeletal muscle, respectively [13]. Previous studies reported that metformin had an inhibitory effect on mitochondrial complex I; and, indeed, an inhibition of mitochondrial complex I has been found to increase the AMP/ATP ratio [7, 14, 15]. AMPK activation by metformin was therefore thought to be also mediated by an increase in the AMP/ATP ratio. However, recent studies have reported that metformin action may be mediated without a notable inhibition of mitochondrial metabolism [10, 16].

Recently, a possible role of peroxynitrite ($ONOO^-$), a reactive nitrogen species (RNS), in the mechanism of AMPK activation has been investigated. RNS comprises nitric oxide and its secondary substrates; $ONOO^-$ is generated from superoxide anions (O_2^-) and nitric oxide [17]. Zou et al. reported that metformin activates AMPK through $ONOO^-$ in bovine aortic endothelial cells (BAEC) [18]. However, it is unclear whether RNS generation by metformin is involved in its suppression of hepatic gluconeogenesis or whether RNS generation affects metformin's pharmacological action in lowering of fasting blood glucose levels.

To clarify the mechanism of AMPK activation in liver, we used mouse hepatocytes to investigate the involvement of the AMP/ATP ratio and RNS in AMPK activation by metformin compared with rotenone, a representative complex I inhibitor. To determine whether endogenous nitric oxide production is required for metformin action in hepatocytes, we also performed experiments using mice lacking endothelial nitric oxide synthase (eNOS) [18–21]. We demonstrated that $ONOO^-$ plays a critical role in AMPK activation by metformin in liver and that eNOS is required for metformin action in vitro and in vivo.

Methods

Animals Male C57/BL6 (wild-type) mice were obtained from Shimizu (Kyoto, Japan). Male eNOS-deficient (*eNos* [also known as *Nos3*]$^{-/-}$) mice were obtained from Jackson Laboratories (Bar Harbor, ME, USA). Mice were maintained in a temperature-controlled (25±2°C) environment with a 12 h light/dark cycle. The mice had free access to standard laboratory chow and water. All experiments were carried out with mice aged 8 to 10 weeks. The animals were maintained and used in accordance with the Guidelines for Animal Experiments of Kyoto University. All the experiments involving animals were conducted in accordance with the Guidelines for Animal Experiments of Kyoto University and were approved by the Animal Research Committee, Graduate School of Medicine, Kyoto University.

Hepatocyte preparation and culture Mice hepatocytes were isolated by collagenase digestion as described previously [22]. Primary hepatocytes were prepared by seeding in six well type 1 collagen-coated plates at a density of 1.5×10^6 cells in DMEM (low glucose, 5.6 mmol/l) containing 10% (vol./vol.) FBS, 100 nmol/l regular insulin, 50 U/ml penicillin and 50 μg/ml streptomycin. Hepatocytes were then cultured overnight in a humidified atmosphere (5% CO_2) at 37°C.

Glucose production via gluconeogenesis in hepatocytes Gluconeogenesis was measured as described previously with slight modifications [22, 23]. In brief, freshly isolated hepatocytes from mice fasted for 16 h were treated in 24 well plates (7.5×10^5 cells/well) in 0.5 ml KRB buffer (119.4 mmol/l NaCl, 3.7 mmol/l KCl, 2.7 mmol/l $CaCl_2$, 1.3 mmol/l KH_2PO_4, 1.3 mmol/l $MgSO_4$, 24.8 mmol/l $NaHCO_3$) containing 2% (wt/vol.) BSA, 2 mmol/l oleate, 0.24 mmol/l 3-isobutyl-1-methylxanthine and gluconeogenetic substrates (1 mmol/l pyruvate plus 10 mmol/l lactate) treated with metformin (Sigma, St Louis, MO, USA) and rotenone (Nacalai Tesque, Kyoto, Japan). Metformin was dissolved in water. Rotenone was dissolved in dimethyl sulfoxide to a concentration that did not interfere with cell viability (maximally 0.1% vol./vol.).

The glucose content of the supernatant fraction was measured by the glucose oxidation method using an assay kit (Gopod; Megazyme, Wicklow, Ireland). The data were normalised by protein content measured by cell lysates.

Immunoblotting analysis Freshly isolated hepatocytes were treated with metformin, rotenone and $ONOO^-$ (Dojindo, Kumamoto, Japan) in KRB buffer containing 2% (wt/vol.) BSA, 2 mmol/l oleate, 0.24 mmol/l 3-isobutyl-1-methylxanthine and gluconeogenetic substrates (1 mmol/l pyruvate plus 10 mmol/l lactate). Primary hepatocytes cultured overnight were incubated in FBS-free DMEM (no glucose) treated with metformin and rotenone. The hepatocytes were homogenised in lysis buffer (50 mmol/l Tris–HCl, pH 7.4, 50 mmol/l NaF, 1 mmol/l sodium pyrophosphate, 1 mmol/l EDTA, 1 mmol/l EGTA, 1 mmol/l dithiothreitol, 0.1 mmol/l benzamidine, 0.1 mmol/l phenylmethylsulfonylfluoride, 0.2 mmol/l sodium vanadate, 250 mmol/l mannitol, 1% (vol./vol.) Triton X-100 and 5 μg/ml soybean trypsin inhibitor). Cell lysates (50 to 150 μg protein per lane) were subjected to electrophoresis on 8% (vol./vol.) SDS–polyacrylamide gels and transferred on to nitrocellulose membranes (Protran; Schleicher and Schuell, Keene, NH, USA). Blotted membranes were incubated with each primary antibody (1:1,000 dilution). Antibodies against AMPKα and phospho-AMPKα (Thr^{172}) were from Cell Signaling Technology (Danvers, MA, USA). Antibodies against organic cation transporter 1 (OCT1) and glyceraldehyde-3-phosphate dehydrogenase were from Santa Cruz Biotechnology (Santa Cruz, CA, USA). Membranes were incubated with horseradish peroxidase-linked second antibodies (1:2,000 dilution) (GE Healthcare, Tokyo, Japan) and fluorescent bands were visualised using a western blotting detection system (Amersham ECL Plus; GE Healthcare) and then quantified by densitometry using Image J software from National Institutes of Health (Bethesda, MD, USA).

Determination of reactive nitrogen species $ONOO^-$ generation was measured using 2,7-dihydrodichlorofluorescein (DCDHF) diacetate (Cayman Chemical, Ann Arbor, MI, USA) [24–26], which is readily oxidised by $ONOO^-$ to the highly fluorescent product, dichlorofluorescein. Alone, nitric oxide, superoxide anions or hydrogen peroxide did not oxidise DCDHF. Freshly isolated hepatocytes were washed in ice-cold PBS and preloaded for 20 min at 37°C with 10 μmol/l DCDHF diacetate (Cayman Chemical) in KRB buffer containing 2% (wt/vol.) BSA, 2 mmol/l oleate, 0.24 mmol/l 3-isobutyl-1-methylxanthine and gluconeogenetic substrates (1 mmol/l pyruvate plus 10 mmol/l lactate). Fluorescence was determined using a spectrofluorophotometer (RF-5300PC; Shimazu, Kyoto, Japan) with excitation wavelength at 502 nm and emission wavelength at 523 nm. After 1 h incubation in the presence or absence of metformin, rotenone, $ONOO^-$ or hydrogen peroxide with or without RNS scavenger (5 mmol/l α-tocopherol plus 2.3 mmol/l ascorbate) [27], fluorescence was measured and presented as a ratio with respect to the value at time zero.

Immunocytochemistry Primary hepatocytes were plated on cover glass coated with 0.01% (vol./vol.) poly-L-lysine (Sigma) in six-well plates (5.0×10^5 cells per well). Hepatocytes were then incubated with FBS-free DMEM (no glucose) in the presence or absence of rotenone, metformin, metformin with RNS scavenger (5 mmol/l α-tocopherol plus 2.3 mmol/l ascorbate) and metformin with 1 mmol/l of the nitric oxide synthase (NOS) inhibitor N^{ω}-nitro-L-arginine methyl ester (L-NAME) for 2 h, or in the presence or absence of $ONOO^-$ for 5 min. The hepatocytes were fixed in 3.7% (wt/vol.) paraformaldehyde and incubated with rabbit polyclonal anti-nitrotyrosine antibody (1:100 dilution; Millipore; Billerica, MA, USA). Next, cells were incubated with goat anti-rabbit IgG fluorescein-conjugated secondary antibody (1:100 dilution; Alexa Fluor 488; Invitrogen, Carlsbad, CA, USA). Fluorescence in cells was monitored using a laser scanning microscope (LSM 510; Carl Zeiss, Tokyo, Japan) for confocal microscopy and a software package (LSM 510 Meta; Carl Zeiss) for image acquisition.

Measurement of adenine nucleotide content After freshly isolated hepatocytes were incubated in KRB buffer containing 2% (wt/vol.) BSA, 2 mmol/l oleate, 0.24 mmol/l 3-isobutyl-1-methylxanthine and gluconeogenetic substrates (1 mmol/l pyruvate plus 10 mmol/l lactate) in the presence or absence of metformin or rotenone for 2 h, or of $ONOO^-$ for 5 min, treatment was stopped by rapid addition of 0.1 ml of 2 mol/l $HClO_4$, followed by mixing by vortex and sonication in ice-cold water for 3 min. Cell lysates were then centrifuged for 3 min at 3,000×*g* and 4°C, and a fraction (0.4 ml) of the supernatant fraction was mixed with 0.1 ml of 2 mol/l HEPES and 0.1 ml of 1 mol/l Na_2CO_3. Adenine nucleotide contents were measured by a luminometric method as previously described [28, 29].

Effect of metformin on plasma glucose levels and AMPK phosphorylation in liver tissue of wild-type and $eNos^{-/-}$ diabetic mice Mice were made diabetic by intraperitoneal injection of streptozotocin (120 mg/kg) into male C57/BL6 and $eNos^{-/-}$ mice at 8 weeks of age. At 1 week after injection of streptozotocin, the animals were confirmed to be diabetic by high fed blood glucose levels (≥13.8 mmol/l) and other diabetic features, including polyuria, polydispia and hyperphagia. After fasting for 16 h, the blood glucose levels were measured and mice were immediately injected intraperitoneally with metformin (250 mg/kg) in 0.9%

sterile saline or 0.9% (wt/vol.) sterile saline only, a similar treatment to that described previously [8, 18]. Blood glucose levels were measured again after 1 h. Diabetic mice received injections of metformin or vehicle as described above for three consecutive days and blood glucose levels were measured again after fasting for 16 h. Immediately after the final measurement of blood glucose levels, the abdomen was cut open and liver tissue of each group was collected and homogenised in lysis buffer. Tissue lysates (50 μg protein/lane) were used for immunoblotting assay of AMPK phosphorylation using antibodies against AMPKα and phospho-AMPKα (Thr^{172}).

Statistical analysis Results are expressed as mean ± SE per number (n) of animals. Statistical significance was evaluated by ANOVA, unpaired t test (not noted) and paired t test (noted). A value of $p<0.05$ was considered statistically significant.

Results

Effects of metformin and rotenone on gluconeogenesis and AMPKα phosphorylation in C57/BL6 mice hepatocytes Hepatic gluconeogenesis and AMPKα phosphorylation were measured using freshly isolated hepatocytes. After 2 h exposure to metformin, hepatic gluconeogenesis was significantly and dose-dependently suppressed at doses between 0.5 and 50 mmol/l metformin; it was also suppressed by exposure to 100 nmol/l rotenone (control 115.4±2.5 nmol/mg protein, 2 mmol/l metformin 92.1±3.3 nmol/mg protein, $p<0.05$ vs control; 100 nmol/l rotenone 91.5±8.7 nmol/mg protein, $p<0.05$ vs control; Fig. 1a). Gluconeogenesis at 2 mmol/l metformin and 100 nmol/l rotenone were similar (p=NS metformin vs rotenone). After 2 h exposure, metformin (0.5–50 mmol/l) and 100 nmol/l rotenone each stimulated phosphorylation of Thr^{172} of AMPKα (Fig. 1b, c). Increments of phosphorylation relative to control in hepatocytes exposed to 2 mmol/l metformin and 100 nmol/l rotenone were almost equivalent (fold increase relative to control 1.79±0.11 [metformin] and 1.85±0.12 [rotenone], p=NS, metformin vs rotenone). Similar results were observed using primary cultured hepatocytes (Fig. 1d, e). In the time course study of exposure to 2 mmol/l metformin, the suppressing effects on gluconeogenesis appeared after 120 min ($p < 0.05$ vs corresponding control; Fig. 1f). In addition, after 60 min exposure to 2 mmol/l metformin stimulated phosphorylation of Thr^{172} of AMPKα ($p<0.05$ vs pre-exposure; Fig. 1g, h).

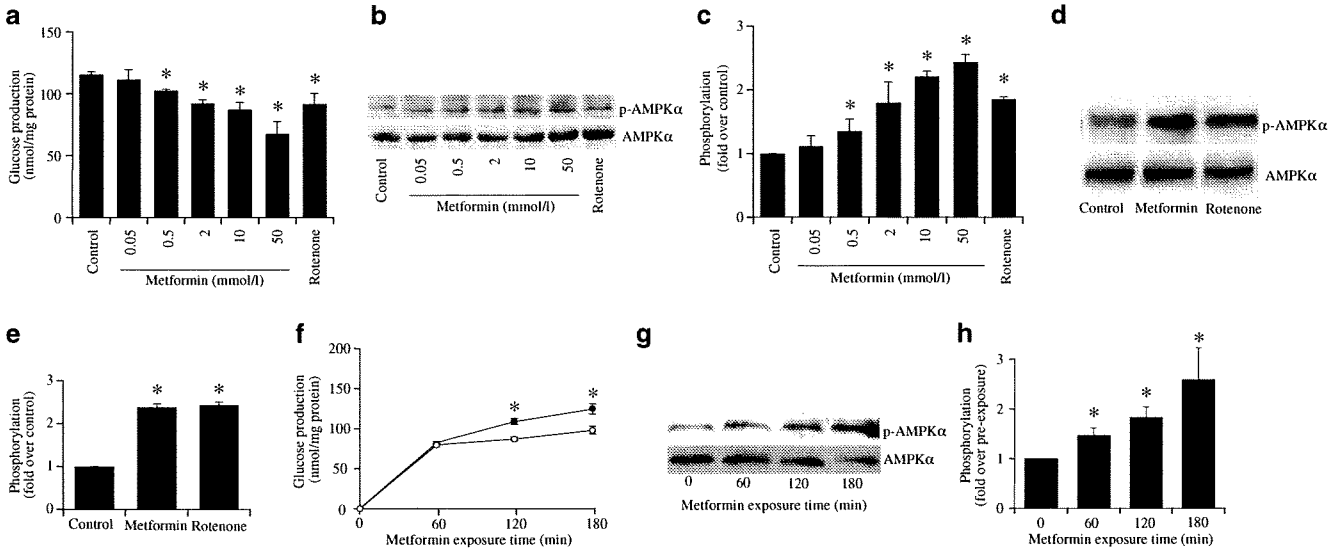

Fig. 1 Metformin and rotenone suppress gluconeogenesis and stimulate AMPKα phosphorylation in hepatocytes isolated from C57/BL6 mice. **a** Gluconeogenesis after 2 h exposure to metformin and rotenone. Metformin (dose-dependently between 0.5 and 50 mmol/l) and rotenone (100 nmol/l) significantly suppressed gluconeogenesis. **b, c** Effects of metformin and rotenone on activation of AMPK. After 2 h exposure, AMPKα phosphorylation in freshly isolated hepatocytes was significantly stimulated by metformin (dose-dependently as above [**a**]) and rotenone (100 nmol/l). Data are expressed as fold stimulation over control. **d, e** Effects of metformin and rotenone on activation of AMPK in primary cultured hepatocytes. After 2 h exposure, AMPKα phosphorylation was significantly stimulated by metformin (2 mmol/l) and rotenone (100 nmol/l). Data are expressed as fold stimulation over control. **f** Time course of gluconeogenesis with exposure to metformin. Suppressing effects on gluconeogenesis by 2 mmol/l metformin (white circles) compared with control (black circles) were detected after 120 min. **g, h** Time course of AMPK activation upon exposure to metformin (2 mmol/l), which after 60 min stimulated phosphorylation of AMPKα in freshly isolated hepatocytes. Data are expressed as fold stimulation over pre-exposure. Values (all bar graphs) are means ± SE (n=6), *$p<0.05$ vs control (**a–f**) and pre-exposure (**h**)

ATP content and AMP/ATP ratio in C57/BL6 mice hepatocytes In wild-type mice, exposure of freshly isolated hepatocytes to 100 nmol/l rotenone for 2 h decreased ATP content and increased the AMP/ATP ratio compared with control (Table 1). However, 2 h exposure to 2 mmol/l metformin did not alter ATP content or AMP/ATP ratio compared with control. ATP content and the AMP/ATP ratio at 2 mmol/l metformin and 100 nmol/l rotenone were significantly different ($p<0.01$ metformin vs rotenone).

RNS production by metformin In freshly isolated hepatocytes, exposure to 2 mmol/l metformin for 1 h increased DCDHF fluorescence, revealing an increase of $ONOO^-$ generation, whereas 300 μmol/l hydrogen peroxide or 100 nmol/l rotenone had no effect on DCDHF fluorescence (Table 2). Co-administration of RNS scavengers (vitamin E plus vitamin C) completely suppressed RNS production by metformin.

Immunocytochemical staining of primary cultured hepatocytes with anti-nitrotyrosine antibody was performed to detect $ONOO^-$ (Fig. 2). $ONOO^-$ (10 μmol/l) incubated for 5 min in primary hepatocytes increased nitrotyrosine staining. Exposure to 2 mmol/l metformin, but not to 100 nmol/l rotenone for 2 h increased nitrotyrosine staining (Fig. 2a). Similarly to the DCDHF fluorescence study, co-administration of RNS scavengers (vitamin E plus vitamin C) suppressed nitrotyrosine staining by metformin. Co-administration of L-NAME, a NOS inhibitor, suppressed $ONOO^-$ generation by metformin (Fig. 2b).

Effect of direct exposure to $ONOO^-$ on AMPKα phosphorylation and AMP/ATP ratio The direct effect of exogenous $ONOO^-$ on AMPK phosphorylation in the absence of metformin was examined. Exposure to $ONOO^-$ for 5 min stimulated phosphorylation of AMPKα by 1 to 100 μmol/l ($p < 0.05$ vs control) (Fig. 3a, b). Exposure to 10 μmol/l $ONOO^-$ for 5 min did not affect ATP content (pre-exposure 0.49±0.05 nmol/mg protein; 5 min $ONOO^-$ 0.50±0.05 nmol/mg protein, p = NS vs pre-exposure, n=5) or the AMP/ATP ratio (pre-exposure 0.99±0.06, 5 min $ONOO^-$ 0.98±0.05, p = NS vs pre-exposure, n=5).

Table 1 Effect of metformin or rotenone on ATP content and AMP/ATP ratio in hepatocytes

Treatments per mouse type	ATP (nmol/mg protein)	AMP/ATP ratio
Wild-type mice		
Control	0.45±0.08	0.98±0.07
Metformin	0.47±0.05	0.96±0.12
Rotenone	0.13±0.02**	1.94±0.13**
eNos$^{-/-}$ mice		
Control	0.42±0.07	1.22±0.11
Metformin	0.41±0.06	1.27±0.16
Rotenone	0.11±0.03**	2.34±0.23**

Values are means ± SE (n=5)

**$p<0.01$ vs control

No effect of metformin on gluconeogenesis, AMPKα phosphorylation or $ONOO^-$ generation in hepatocytes lacking eNOS In freshly isolated hepatocytes from *eNos*$^{-/-}$ mice, 2 h exposure to 2 mmol/l metformin did not suppress gluconeogenesis, whereas exposure to 100 nmol/l rotenone suppressed gluconeogenesis to a similar degree to that observed in wild-type hepatocytes (control 110.1±4.4 nmol/mg protein, metformin 107.0±3.9 nmol/mg protein, p=NS vs control; rotenone 81.6±8.8 nmol/mg protein, $p<0.05$ vs control; Fig. 4a). Metformin did not stimulate AMPKα phosphorylation in freshly isolated hepatocytes from *eNos*$^{-/-}$ mice, whereas rotenone significantly stimulated AMPKα phosphorylation (fold increase relative to control at 2 h: metformin 0.96±0.12, p=NS vs control; rotenone 1.94±0.13, $p<0.05$ vs control; Fig. 4b, c). Similarly, in primary cultured hepatocytes, metformin also did not stimulate, whereas rotenone significantly stimulated AMPKα phosphorylation (Fig. 4d, e). Metformin also did not increase nitrotyrosine staining in primary cultured hepatocytes from *eNos*$^{-/-}$ mice, indicating no generation of $ONOO^-$ (Fig. 4f). In addition, nitrotyrosine staining was not induced by 2 h exposure to rotenone. Exposure of *eNos*$^{-/-}$ freshly isolated hepatocytes to 100 nmol/l rotenone also decreased ATP content and increased the AMP/ATP ratio, whereas exposure to metformin had not effect (Table 1). Recently, it was reported that metformin is first transported across the plasma membrane before exerting its cellular action, a step mediated by OCT1 [30]. To exclude involvement of OCT1 in *eNos*$^{-/-}$ mice, we confirmed that levels of OCT1 protein in freshly isolated hepatocytes from *eNos*$^{-/-}$ mice were similar to those in wild-type mice hepatocytes (Fig. 4g).

Essential role of eNOS in lowering of glucose levels by metformin in diabetic mice in vivo To determine whether metformin lowers fasting blood glucose levels in the absence of eNOS, metformin (250 mg/kg) was injected intraperitoneally into streptozotocin-induced diabetic wild-type or *eNos*$^{-/-}$ mice. Characteristics of wild-type and *eNos*$^{-/-}$ mice used in the experiments showed no significant differences in body weight, fasting blood glucose levels or fed blood glucose levels before streptozotocin injection at 8 weeks of age among the four groups (Table 3).

Fasting blood glucose levels were lowered by about 3.9 mmol/l at 1 h after single administration of metformin in overnight-fasted wild-type diabetic mice, whereas those in overnight-fasted *eNos*$^{-/-}$ diabetic mice were not altered

Table 2 Effect of metformin on RNS production

Treatments	No addition	Addition of vitamins E and C
Control	1.03±0.01	0.94±0.01**
Metformin (2 mmol/l)	1.15±0.04*	0.95±0.01**
Rotenone (100 nmol/l)	1.03±0.02	0.99±0.01**
Hydrogen peroxide (300 μmol/l)	1.02±0.02	0.98±0.01**
$ONOO^-$ (10 μmol/l)	1.21±0.05*	1.00±0.01**

Data are expressed as the value at 60 min divided by the value at time zero (fold increase); values are means ± SE (n=8)

*p<0.05 vs control; **p<0.01 vs corresponding values without RNS scavengers

(Table 3). Administration of vehicle (saline) alone in overnight-fasted wild-type diabetic mice did not alter fasting blood glucose levels after single administration, as was also found in overnight-fasted *eNos*$^{-/-}$ diabetic mice (Table 3). Following the first injection, daily administration of metformin was continued for two more days. Administration of metformin for three consecutive days lowered fasting blood glucose levels by about 7.1 mmol/l in wild-type diabetic mice, whereas it had no lowering effect on fasting blood glucose in diabetic *eNos*$^{-/-}$ mice (Table 3). Administration of vehicle (saline) alone in overnight-fasted wild-type mice did not alter fasting blood glucose levels after administration for three consecutive days, as was also the case in *eNos*$^{-/-}$ mice (Table 3).

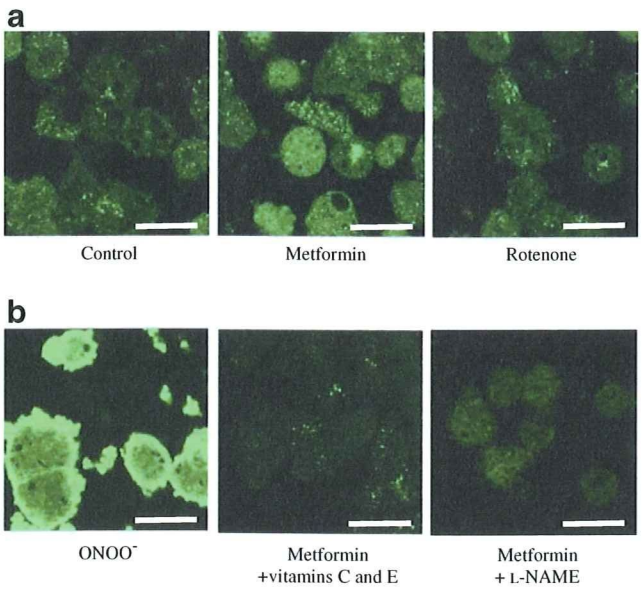

Fig. 2 Immunocytochemical staining with anti-nitrotyrosine antibody for detection of $ONOO^-$ generation. $ONOO^-$ (10 μmol/l) incubated for 5 min was used as a positive control. **a** Exposure to metformin (2 mmol/l) for 2 h increased staining, but exposure to rotenone (100 nmol/l) for the same time did not. **b** $ONOO^-$ generation induced by metformin was decreased by co-administration with RNS scavengers (5 mmol/l α-tocopherol [vitamin E] plus 2.3 mmol/l ascorbate [vitamin C]) and a NOS inhibitor (1 mmol/l L-NAME), respectively. Confocal microscopy, magnifications ×100; scale bars 50 μm

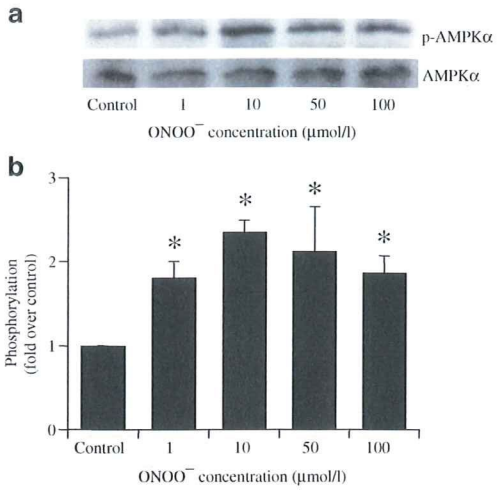

Fig. 3 Exogenous $ONOO^-$ stimulates AMPKα phosphorylation in freshly isolated hepatocytes. **a** Blot showing that direct exposure to $ONOO^-$ for 5 min at doses ranging from 1 to 100 μmol/l stimulated AMPKα phosphorylation. **b** Quantification with data expressed as fold stimulation over control. Values are means ± SE (n=4), *p<0.05 vs control

Lack of effects of metformin in vivo on AMPKα phosphorylation in liver tissues lacking eNOS In liver tissue samples collected after three consecutive days of administration, metformin stimulated phosphorylation of AMPKα in wild-type mice (metformin 2.17±0.30 [fold increase relative to vehicle], p<0.05 vs vehicle; Fig. 5a, b). However, stimulation of AMPKα phosphorylation by metformin was not observed in liver tissues of *eNos*$^{-/-}$ mice (metformin 0.97±0.12 [fold increase relative to vehicle], p=NS vs saline; Fig. 5a, c).

Discussion

In the present study, we show for the first time that activation of AMPK and the inhibitory effect on hepatic gluconeogenesis by metformin are mediated by generation of the RNS, $ONOO^-$. We also showed that eNOS plays an important role in metformin action in liver.

We investigated the metformin–RNS–AMPK pathway for its suppressing effects on hepatic gluconeogenesis. Because recent studies have shown that metformin activates AMPK through the RNS, $ONOO^-$, in BAEC [18], we evaluated RNS production in liver, the major target of metformin action. We found that metformin increased $ONOO^-$ generation and that $ONOO^-$ itself activates AMPK, which is induced in only 5 min. A previous study found that AMPK phosphorylation by metformin does not appear within 10 min but only after 30 min [31]. Consistent

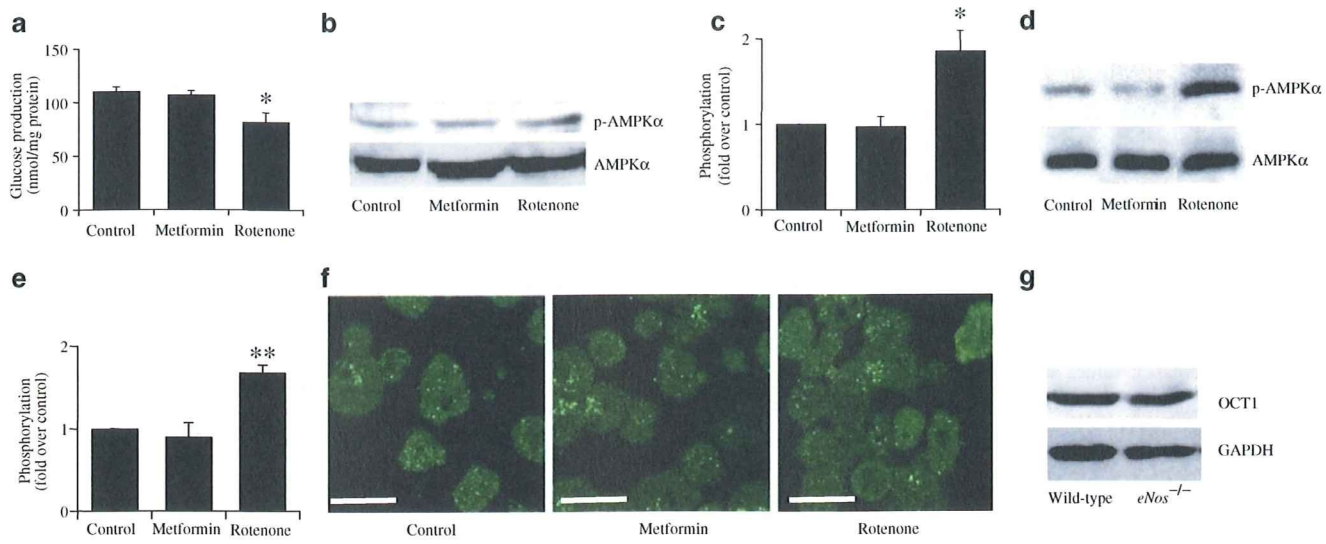

Fig. 4 Lack of effects of metformin on suppression of gluconeogenesis, AMPKα phosphorylation and $ONOO^-$ generation in hepatocytes lacking eNOS. **a** Metformin (2 mmol/l) did not suppress gluconeogenesis after 2 h exposure in hepatocytes lacking eNOS, but rotenone (100 nmol/l) suppressed gluconeogenesis to a similar degree to that observed in wild-type hepatocytes. Values are means ± SE (n=6), *p< 0.05 vs control. **b** Blot showing that AMPKα phosphorylation was not stimulated by metformin (2 mmol/l), but was stimulated by rotenone (100 nmol/l) after 2 h exposure in freshly isolated hepatocytes; (**c**) quantification with data expressed as fold stimulation over control. Values are means ± SE (n=4), *p<0.05 vs control. **d** Blot showing that AMPKα phosphorylation was not stimulated by metformin (2 mmol/l), but was stimulated by rotenone (100 nmol/l) after 2 h exposure in primary cultured hepatocytes, with (**e**) bar graph showing data expressed as fold stimulation over control. Values are means ± SE (n=5), **p<0.01 vs control. **f** Immunocytochemical staining (confocal microscopy) with anti-nitrotyrosine antibody in hepatocytes lacking eNOS. Exposure to metformin (2 mmol/l) and rotenone (100 nmol/l) for 2 h did not increase staining. Magnification ×100, scale bar 50 μm. **g** Levels of OCT1 protein in wild-type and *eNos*$^{-/-}$ mice hepatocytes. OCT1 levels in *eNos*$^{-/-}$ mice hepatocytes were similar to those in wild-type mice hepatocytes. Findings normalised to glyceraldehyde-3-phosphate dehydrogenase (GAPDH)

with that study, our data showed that AMPK phosphorylation by metformin did not appear within 15 min, but only after more than 30 min (data not shown). Thus, $ONOO^-$ generation appears to precede AMPK phosphorylation after exposure to metformin. $ONOO^-$ is generated by nitric oxide and superoxide anions; intra-hepatocellular nitric oxide is produced by NOS. In the present study, the NOS inhibitor, L-NAME, suppressed $ONOO^-$ production by metformin. This suggests that nitric oxide production by hepatocellular NOS is required for $ONOO^-$ production by metformin. Since eNOS is the representative subtype of the NOS family for generation of $ONOO^-$ in liver [17], we sought to determine whether eNOS is required for $ONOO^-$ production by metformin. Using eNOS-deficient mice, we were able to demonstrate that eNOS is essential for metformin action in liver. Thus metformin increases $ONOO^-$ produc-

Table 3 Effect of metformin on blood glucose levels in wild-type and *eNos*$^{-/-}$ diabetic mice

Treatments per mouse type	Pre streptozotocin			Post streptozotocin		
	Body weight (g)	FBG (mmol/l)	Fed BG (mmol/l)	FBG (mmol/l)	BG (mmol/l) at 1 h PM	FBG (mmol/l) after 3 days met
Wild-type mice						
Saline	20.3±0.4	3.7±0.2	8.2±0.5	16.0±2.7	17.2±3.1	16.6±3.3
Metformin	20.4±0.3	3.7±0.2	8.0±0.3	16.6±2.8	12.7±3.0**	9.5±1.9**
eNos$^{-/-}$ mice						
Saline	20.5±0.3	3.6±0.2	7.9±0.4	15.0±1.9	17.3±2.4	16.9±2.7
Metformin	20.7±0.3	3.5±0.2	8.1±0.5	15.8±1.6	19.0±1.9	16.5±2.1

Values are means ± SE (n=8)

**p<0.01 vs the value of pre-injection intraperitoneally with metformin in saline or saline only, paired t test

BG, blood glucose; FBG, fasting blood glucose; met, metformin; PM, post-metformin

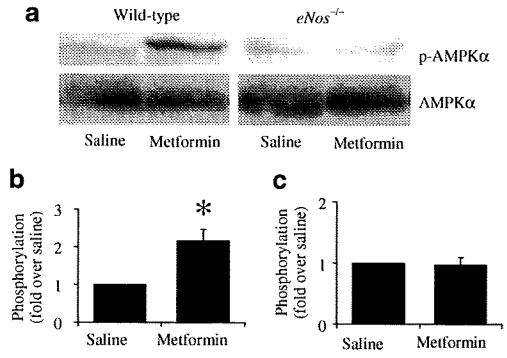

Fig. 5 Lack of effects of metformin in vivo on AMPKα phosphorylation in liver tissues deficient in eNOS. **a** Blot showing that metformin stimulated phosphorylation of AMPKα in liver tissues of wild-type diabetic mice after administration for three consecutive days. **b** Quantification of blot for wild-type and (**c**) *eNos*$^{-/-}$ mice. Metformin did not stimulate (**a, c**) phosphorylation of AMPKα in liver tissues of *eNos*$^{-/-}$ diabetic mice after metformin administration for three consecutive days. Data (**b, c**) are expressed as fold stimulation over saline. Values are means ± SE (n=5), *p<0.05 vs vehicle

tion, which is followed by AMPK activation and suppression of gluconeogenesis.

Although metformin has been reported not to affect the ATP content of hepatocytes [32], several studies have found that metformin decreased ATP content and/or increased the AMP/ATP ratio in hepatocytes [23, 33], possibly a result of metformin's suppressive effect on complex I activity in the respiratory chain [34] and one that plays an important role in AMPK activation by metformin. While metformin was found not to affect ATP content and the AMP/ATP ratio in the present study, the AMP/ATP ratio might nevertheless play an important role in AMPK activation by metformin because AMPK is sensitive to changes in the AMP/ATP ratio at levels too slight to be detected by measurement of the total adenine nucleotide content of whole cells [35]. Interestingly, metformin activates AMPK with a smaller increase in the AMP/ATP ratio than that effected by mitochondrial uncoupler and rosiglitazone [16] and without affecting the ADP/ATP ratio [10]. These results suggest that, apart from increases in the AMP/ATP ratio, other important mechanisms may be involved in AMP activation by metformin.

Rotenone inhibits complex I of the mitochondrial respiratory chain and decreases oxidative phosphorylation, leading to ATP depletion and an increase in the AMP/ATP ratio, which results in stimulation of AMPK phosphorylation. In the present study we observed that while 2 mmol/l metformin and 100 nmol/l rotenone had similar effects on gluconeogenesis and AMPK phosphorylation, the AMP/ATP ratio increased prominently only upon exposure to rotenone but not upon exposure to metformin. These results indicate that complex I inhibition alone is unlikely to explain the action of metformin. Interestingly, metformin significantly increased RNS in contrast to the lack of effect of rotenone on RNS. Furthermore, a decrease in metformin-induced RNS production by eNOS disruption abolished activation of AMPK by metformin. These results demonstrate that RNS is a regulator distinct from the AMP/ATP ratio in AMPK activation by metformin.

Some groups have reported that eNOS acts upstream of AMPK activation in BAEC [18], while other groups have reported that eNOS acts downstream of AMPK activation in capillary endothelial cells and in cardiomyocytes [21]. In the present study, we show that, in wild-type hepatocytes, direct exposure to $ONOO^-$ activates AMPK and that rotenone activates AMPK without increase in $ONOO^-$ production, supporting the former notion [18] in hepatocytes.

It is well known that high levels of RNS have deleterious effects on cell function and viability [17]. On the other hand, the low levels of RNS seen in physiological conditions are required for maintaining normal cell functions such as signal transduction [36]. For example, it has been reported that RNS production induced by skeletal muscle contraction is correlated with glucose uptake [20]. Thus, RNS has protective and damaging effects on cells. Indeed, the RNS produced by metformin at a dose used in the present study (2 mmol/l) should have beneficial effects on hepatic glucose metabolism through AMPK activation.

We demonstrate in the present study that AMPK activation by metformin in hepatocytes is dependent on RNS. We also demonstrate that eNOS plays an important role in suppressing hepatic gluconeogenesis in vitro as well as in lowering fasting blood glucose levels in vivo. It is generally accepted that fasting blood glucose levels are determined by hepatic gluconeogenesis, which suggests that eNOS is required for metformin's action on fasting blood glucose levels.

In the present study, we have elucidated a novel mechanism for metformin action. However, some limitations of this study must be considered. In our in vivo metformin experiments, the mice were injected intraperitoneally with 250 mg/kg metformin in 0.9% sterile saline, which is a similar dosage to that used previously [8, 18]. This protocol using a high dose of metformin for rodents may cause a very distinct acute response. Therefore, we cannot exclude the possibility that the acute hepatocellular response to AMPK activation by metformin in the present study differs from the clinical effects of metformin when used to treat patients with type 2 diabetes. To elucidate the detailed mechanisms of AMPK activation by metformin in liver, which may provide novel therapeutic targets for type 2 diabetes, further investigations are required.

Acknowledgements This study was supported by Scientific Research Grants, a Grant for Leading Project for Biosimulation from the Ministry of Education, Culture, Sports, Science and Technology of Japan, and by a grant from CREST of Japan Science and Technology Cooperation. Support was also provided in the form of a grant from the Ministry of Health, Labor and Welfare, Japan, and also by Kyoto University Global COE Program 'Center for Frontier Medicine'.

Duality of interest The authors declare that there is no duality of interest associated with this manuscript.

References

1. Nathan DM, Buse JB, Davidson MB et al (2008) Management of hyperglycaemia in type 2 diabetes mellitus: a consensus algorithm for the initiation and adjustment of therapy. Update regarding the thiazolidinediones. Diabetologia 51:8–11
2. Nathan DM, Buse JB, Davidson MB et al (2006) Management of hyperglycaemia in type 2 diabetes: a consensus algorithm for the initiation and adjustment of therapy. A consensus statement from the American Diabetes Association and the European Association for the Study of Diabetes. Diabetologia 49:1711–1721
3. Inzucchi SE, Maggs DG, Spollett GR et al (1998) Efficacy and metabolic effects of metformin and troglitazone in type II diabetes mellitus. N Engl J Med 338:867–873
4. Scarpello JH, Howlett HC (2008) Metformin therapy and clinical uses. Diab Vasc Dis Res 5:157–167
5. Bailey CJ (1992) Biguanides and NIDDM. Diabetes Care 15:755–772
6. UK Prospective Diabetes Study (UKPDS) Group (1998) Effect of intensive blood-glucose control with metformin on complications in overweight patients with type 2 diabetes (UKPDS 34). Lancet 352:854–865
7. Brunmair B, Staniek K, Gras F et al (2004) Thiazolidinediones, like metformin, inhibit respiratory complex I. Diabetes 53:1052–1059
8. Shaw RJ, Lamia KA, Vasquez D et al (2005) The kinase LKB1 mediates glucose homeostasis in liver and therapeutic effects of metformin. Science 310:1642–1646
9. Zhou G, Myers R, Li Y, Chen Y et al (2001) Role of AMP-activated protein kinase in mechanism of metformin action. J Clin Invest 108:1167–1174
10. Hawley SA, Gadalla AE, Olsen GS, Hardie DG (2002) The antidiabetic drug metformin activates the AMP-activated protein kinase cascade via an adenine nucleotide-independent mechanism. Diabetes 51:2420–2425
11. Tian R, Musi N, D'Agostino J, Hirshman MF, Goodyear LJ (2001) Increased adenosine monophosphate-activated protein kinase activity in rat hearts with pressure-overload hypertrophy. Circulation 104:1664–1669
12. Hardie DG (2004) The AMP-activated protein kinase pathway—new players upstream and downstream. J Cell Sci 117:5479–5487
13. Hardie DG, Hawley SA, Scott JW (2006) AMP-activated protein kinase—development of the energy sensor concept. J Physiol 574: 7–15
14. El-Mir MY, Nogueira V, Fontaine E, Ave'ret N, Rigoulet M, Leverve X (2000) Dimethylbiguanide inhibits cell respiration via an indirect effect targeted on the respiratory chain complex I. J Biol Chem 275:223–228
15. Owen MR, Doran E, Halestrap AP (2000) Evidence that metformin exerts its anti-diabetic effects through inhibition of complex 1 of the mitochondrial respiratory chain. Biochem J 348:607–614
16. Fryer LG, Parbu-Patel A, Carling D (2002) The anti-diabetic drugs rosiglitazone and metformin stimulate AMP-activated protein kinase through distinct signaling pathways. J Biol Chem 277:25226–25232
17. Pacher P, Beckman JS, Liaudet L (2007) Nitric oxide and $ONOO^-$ in health and disease. Physiol Rev 87:315–424
18. Zou MH, Kirkpatrick SS, Davis BJ et al (2004) Activation of the AMP-activated protein kinase by the anti-diabetic drug metformin in vivo. Role of mitochondrial reactive nitrogen species. J Biol Chem 279:43940–43951
19. Davis BJ, Xie Z, Viollet B, Zou MH (2006) Activation of the AMP-activated kinase by antidiabetes drug metformin stimulates nitric oxide synthesis in vivo by promoting the association of heat shock protein 90 and endothelial nitric oxide synthase. Diabetes 55:496–505
20. Ross RM, Wadley GD, Clark MG, Rattigan S, McConell GK (2007) Local nitric oxide synthase inhibition reduces skeletal muscle glucose uptake but not capillary blood flow during in situ muscle contraction in rats. Diabetes 56:2885–2892
21. Chen ZP, Mitchelhill KI, Michell BJ et al (1999) AMP-activated protein kinase phosphorylation of endothelial NO synthase. FEBS Lett 443:285–289
22. Fujiwara H, Hosokawa M, Zhou X et al (2008) Curcumin inhibits glucose production in isolated mice hepatocytes. Diabetes Res Clin Pract 80:185–191
23. Argaud D, Roth H, Wiernsperger N, Leverve XM (1993) Metformin decreases gluconeogenesis by enhancing the pyruvate kinase flux in isolated rat hepatocytes. Eur J Biochem 213:1341–1348
24. Kooy NW, Royall JA, Ischiropoulos H (1997) Oxidation of 2′,7′-dichlorofluorescin by $ONOO^-$. Free Radic Res 27:245–254
25. Crow JP (1997) Dichlorodihydrofluorescein and dihydrorhodamine 123 are sensitive indicators of $ONOO^-$ in vitro: implications for intracellular measurement of reactive nitrogen and oxygen species. Nitric Oxide 2:145–157
26. Possel H, Noack H, Augustin W, Keilhoff G, Wolf G (1997) 2,7-Dihydrodichlorofluorescein diacetate as a fluorescent marker for $ONOO^-$ formation. FEBS Lett 416:175–178
27. Kominato R, Fujimoto S, Mukai E et al (2008) Src activation generates reactive oxygen species and impairs metabolism-secretion coupling in diabetic Goto–Kakizaki and ouabain-treated rat pancreatic islets. Diabetologia 51:1226–1235
28. Nabe K, Fujimoto S, Shimodahira M et al (2006) Diphenylhydantoin suppresses glucose-induced insulin release by decreasing cytoplasmic H^+ concentration in pancreatic islets. Endocrinology 147:2717–2727
29. Fujimoto S, Mukai E, Hamamoto Y et al (2002) Prior exposure to high glucose augments depolarization-induced insulin release by mitigating the decline of ATP level in rat islets. Endocrinology 143:213–221
30. Shu Y, Sheardown SA, Brown C et al (2007) Effect of genetic variation in the organic cation transporter 1 (OCT1) on metformin action. J Clin Invest 117:1422–1431
31. Xie Z, Dong Y, Scholz R, Neumann D, Zou MH (2008) Phosphorylation of LKB1 at serine 428 by protein kinase C-ζ is required for metformin-enhanced activation of the AMP-activated protein kinase in endothelial cells. Circulation 117: 952–962
32. Wollen N, Bailey CJ (1988) Inhibition of hepatic gluconeogenesis by metformin. Synergism with insulin. Biochem Pharmacol 37:4353–4358
33. Guigas B, Bertrand L, Taleux N et al (2006) 5-Aminoimidazole-4-carboxamide-1-beta-D-ribofuranoside and metformin inhibit

hepatic glucose phosphorylation by an AMP-activated protein kinase-independent effect on glucokinase translocation. Diabetes 55:865–874
34. Hinke SA, Martens GA, Cai Y et al (2007) Methyl succinate antagonises biguanide-induced AMPK-activation and death of pancreatic beta-cells through restoration of mitochondrial electron transfer. Br J Pharmacol 150:1031–1043
35. Zhang L, He H, Balschi JA (2007) Metformin and phenformin activate AMP-activated protein kinase in the heart by increasing cytosolic AMP concentration. Am J Physiol Heart Circ Physiol 293:H457–H466
36. Bashan N, Kovsan J, Kachko I, Ovadia H, Rudich A (2009) Positive and negative regulation of insulin signaling by reactive oxygen and nitrogen species. Physiol Rev 89:27–71

Biochemical and Biophysical Research Communications 393 (2010) 73–78

Contents lists available at ScienceDirect

Biochemical and Biophysical Research Communications

journal homepage: www.elsevier.com/locate/ybbrc

Overexpression of SIRT5 confirms its involvement in deacetylation and activation of carbamoyl phosphate synthetase 1

Masahito Ogura, Yasuhiko Nakamura, Daisuke Tanaka, Xiaotong Zhuang, Yoshihito Fujita, Akio Obara, Akihiro Hamasaki, Masaya Hosokawa, Nobuya Inagaki *

Department of Diabetes and Clinical Nutrition, Graduate School of Medicine, Kyoto University, 54 Kawahara-cho, Shogoin, Sakyo-ku, Kyoto 606–8507, Japan

ARTICLE INFO

Article history:
Received 18 January 2010
Available online 25 January 2010

Keywords:
SIRT5
Mitochondria
Urea cycle
Liver

ABSTRACT

SIR2 protein, an NAD-dependent deacetylase, is localized to nucleus and is involved in life span extension by calorie restriction in yeast. In mammals, among the seven SIR2 homologues (SIRT1-7), SIRT3, 4, and 5 are localized to mitochondria. As SIRT5 mRNA levels in liver are increased by fasting, the physiological role of SIRT5 was investigated in liver of SIRT5-overexpressing transgenic (SIRT5 Tg) mice. We identified carbamoyl phosphate synthetase 1 (CPS1), a key enzyme of the urea cycle that catalyzes condensation of ammonia with bicarbonate to form carbamoyl phosphate, as a target of SIRT5 by two-dimensional electrophoresis comparing mitochondrial proteins in livers of SIRT5 Tg and wild-type mice. CPS1 protein was more deacetylated and activated in liver of SIRT5 Tg mice than in wild-type. In addition, urea production was upregulated in hepatocytes of SIRT5 Tg mice. These results agree with those of a previous study using SIRT5 knockout (KO) mice. Because ammonia generated during fasting is toxic, SIRT5 protein might play a protective role by converting ammonia to non-toxic urea through deacetylation and activation of CPS1.

Introduction

SIR2 protein is an NAD-dependent deacetylase [1]. In yeast, increasing the dosage of the SIR2 gene extends life span, whereas disruption of the SIR2 gene shortens it [2]. SIR2 determines life span not only in yeast but also in *Caenorhabditis elegans* [3] and *Drosophila melanogaster* [4]. Mammals have seven SIR2 homologues, SIRT1-7 [5]. SIRT1 deacetylates and regulates the activities of many proteins in the nucleus. SIRT1 upregulates expression of gluconeogenic genes and downregulates glycolytic genes through deacetylation of PPARγ coactivator-1α and FOXO1 [6,7].

SIRT3, SIRT4, and SIRT5 proteins are known to be localized to mitochondria [8]. *In vitro*, SIRT3 protein deacetylates and activates mitochondrial enzymes such as glutamate dehydrogenase, isocitrate dehydrogenase 2, and acetyl CoA synthetase 2 (AceCS2) [9–11]. While SIRT4 does not have NAD-dependent deacetylase activity, it does have ADP-ribosyl transferase activity. SIRT4 inhibits insulin secretion by repression of glutamate dehydrogenase activity through ADP-ribosylation [12,13]. SIRT5 protein also exhibits NAD-dependent deacetylase activity on histone H4 peptide *in vitro* [13]. Recently, Nakagawa et al. reported that SIRT5 interacts with carbamoyl phosphate synthetase 1 (CPS1), and that deacetylated CPS1 is decreased and CPS1 activity is downregulated in livers of SIRT5 knockout (KO) mice [14].

During fasting or starvation, circulating amino acids are derived mainly from catabolism of skeletal muscle, and are used in gluconeogenesis in liver to maintain blood glucose levels. The ammonia co-generated in liver from these amino acids is toxic; the urea cycle detoxifies this ammonia by converting it to non-toxic, water-soluble urea, which is readily excreted from kidney [15,16].

CPS1 is the mitochondrial protein that catalyzes the first step of the urea cycle, the condensation of ammonia with bicarbonate to form carbamoyl phosphate [15,16]. Patients with CPS1 deficiency exhibit lethally severe hyperammonemia in the neonatal period [16], which suggests a critical role for CPS1 in the urea cycle.

In the present study, to investigate the physiological role of SIRT5, we generated SIRT5-overexpressing transgenic (SIRT5 Tg) mice and attempted to identify the target protein of SIRT5 regulation in liver. We show here that SIRT5 protein might regulate urea production by deacetylation and activation of mitochondrial CPS1, complementing the previous study of SIRT5 KO mice [14].

Materials and methods

Animal Experiments: The mice were housed in an air-controlled (temperature 25 °C) room with dark–light cycle (10 h; 14 h).

Abbreviations: SIR2, silent information regulator 2; CPS1, carbamoyl phosphate synthetase 1; Tg, transgenic; KO, knockout.

* Corresponding author. Fax: +81 75 771 6601.
E-mail address: inagaki@metab.kuhp.kyoto-u.ac.jp (N. Inagaki).

0006-291X/$ - see front matter © 2010 Elsevier Inc. All rights reserved.
doi:10.1016/j.bbrc.2010.01.081

Animal care and procedures were approved by the Animal Care Committee of Kyoto University.

Isolation of total RNA and quantitative RT-PCR: Total RNA was isolated from livers, kidneys and hearts of 11 week-old C57BL/6 mice using Trizol (Invitrogen), and cDNA was prepared by reverse transcriptase (Superscript II; Invitrogen) with an oligo (dT) primer. SIRT5 mRNA levels were measured by real-time quantitative RT-PCR using ABI PRISM 7000 Sequence Detection System (Applied Biosystems). SIRT5 mRNA levels were corrected for β-actin mRNA levels. The mouse sequences of forward and reverse primers to evaluate SIRT5 expression were 5′-GTCATCACCCAGAACATCGA-3′ and 5′-ACGTGAGGTCGCAGCAAGCC-3′; respectively. The mouse sequences of forward and reverse primers to evaluate β-actin expression were 5′-TTGCAGCTCCTTCGTTGC-3′ and 5′-CACGAT GGAGGGGAATACAG-3′, respectively. SYBR Green PCR Master Mix (Applied Biosystems) was prepared for PCR run. The thermal cycling conditions were denaturation at 95 °C for 10 min followed by 50 cycles at 95 °C for 15 s and 60 °C for 1 min.

Plasmid construction: The expression vectors for SIRT5 protein with (pCMV5aSIRT5-FLAG) and without (pCMV5aSIRT5) FLAG tag at the C-terminus were constructed as follows. The coding region of mouse SIRT5 cDNA was cloned by PCR using mouse liver cDNA prepared as described above. The PCR fragments were subcloned into pFLAG-CMV-5a (Sigma).

Antibody: SIRT5 polyclonal antibody was produced by immunizing a rabbit with synthetic peptide CGKTLPEALAPHETE, corresponding to 15 C-terminal amino acid residues of mouse SIRT5 protein. The antibody was purified by HiTrap NHS-activated HP kit (GE Healthcare) and gel filtration column. Western blotting analysis was performed using the obtained anti-SIRT5 or anti-FLAG (Sigma) antibodies.

Generation of SIRT5-overexpressing transgenic mice: SIRT5 cDNA with FLAG tag sequences was inserted to the *Eco*RI site of transgenic plasmid pIns-1 [17], and the human insulin promoter of pIns-1 was then replaced by the CAG promoter derived from pCAGGS plasmid [18]. The transgene cassettes were excised from the resulting plasmid by digestion with *Not*I and *Xho*I, and the linearized cassettes were microinjected to fertilized eggs of C57BL/6 inbred mice (PhoenixBio CO., Ltd. Hiroshima, Japan). Since the two lines revealed similar data, all additional experiments were performed using line #38.

Preparation of mitochondria: The livers of C57BL/6 mice were homogenized in isotonic buffer (PBS containing 0.25 M sucrose) containing protease inhibitors (Complete, EDTA free: Roche) with potter homogenizer. The mitochondria were prepared as described previously [8].

Two-dimensional electrophoresis and identification of protein: Liver mitochondria were prepared as described previously [8] and lysed with rehydration buffer (8 M urea, 2% CHAPS, 50 mM DTT, 0.2% Bio-Lyte (BIO-RAD), 0.001% bromophenol blue), and applied to ReadyStrip IPG Strip (BIO-RAD) and separated by isoelectric focusing electrophoresis with a range pH 5 to pH 8 using PROTEAN IEF cell (BIO-RAD). The IPG Strip was then subjected to SDS–polyacrylamide gel electrophoresis. The obtained gel was stained with SYPRO Ruby protein gel stain kit (invitrogen), and the protein was visualized and analyzed using Typhoon 9210 (GE healthcare). The protein at the indicated spot was isolated and analyzed using MALDI-TOF-MS (APRO Life Science Institute, Inc.).

Immunoprecipitation: Mitochondria lysed with PBS containing 1% Triton X-100 were incubated with anti-CPS1 (Santa Cruz) or anti-acetylated lysine (Cell Signaling) antibody for 16 h at 4 °C. Protein G Sepharose (GE healthcare) was then added and incubation was continued for 3 h. The resin was washed and boiled with SDS sample buffer (0.2 M Tris, 10% sucrose, 10% SDS, 5 mM EDTA). The sample was analyzed by western blotting with anti-CPS1 antibody.

Determination of CPS1 activity: Livers of 8–12 week-old SIRT5 Tg and wild-type mice fasted for 16 h were homogenized [19] and CPS1 activities were assayed as described by Fahien and Cohen [20]. Briefly, the reaction was started by adding the supernatant obtained above (enzyme source) to the assay mixture containing 2.5 mM phosphoenopyruvate, 0.2 mM NADH, 10 mM NH_4Cl, 100 mM $KHCO_3$, 5 mM ATP, 10 mM $MgSO_4$, 10 mM *N*-acetylglutamate, 10 U/ml pyruvate kinase (SIGMA), 12.5 U/ml of lactate dehydrogenase (SIGMA), and 50 mM glycylglycine (pH 7.6) at room temperature, and the decrease in absorbance at 340 nm was measured. The initial velocity of the reaction was directly proportional CPS1 activity. One unit of CPS1 activity corresponded to oxidation of 1 μmol of NADH/min at room temperature.

Measurement of hepatic urea production: Hepatocytes of 8–12 week-old SIRT5 Tg and wild-type mice fasted for 16 h were isolated as described previously [21]. Obtained hepatocytes (1.5×10^5) were incubated at 37 °C in humidified atmosphere (5% CO_2) in 2 ml Krebs ringer buffer with 25 mM $NaHCO_3$, 10 mM NH_4Cl, and 5 mM ornithin–HCl [22]. Incubation was stopped by placing the cells on ice, followed by centrifugation at 4 °C for 10 min at 600*g*. The supernatant was removed and urea concentration was measured by diacetyl monoxime methods [23,24], the cells were lysed with 0.1% SDS, and the protein concentration was determined (Bio-Rad Protein Assay Kit).

Statistical analysis: Values are expressed as means ± SEM. Statistical analysis was performed unpaired Student's *t*-test. *P* values <0.05 were considered significant.

Results

Upregulation of SIRT5 mRNA levels by fasting

Expression levels of SIRT1 mRNA are known to be increased in liver and heart by fasting [25]. However, it is unclear whether the expression levels of SIRT5 are regulated by nutrient conditions. To evaluate alteration of SIRT5 mRNA expression levels in different nutrient conditions, total RNA was extracted from organs including liver, kidney, and heart in C57BL/6 mice fed *ad libitum*, fasted for 24 h, or refed for 24 h after 24-h fasting, and quantitative RT-PCR was carried out. SIRT5 mRNA levels in liver were increased 2.4-fold by fasting ($N = 4$, $P < 0.01$) and were decreased to fed condition levels by refeeding ($N = 4$, $P < 0.05$), but were unchanged in kidney or heart (Fig. 1), suggesting an important role of SIRT5 in liver.

Generation of SIRT5 Tg mice

To clarify the function of SIRT5 *in vivo*, we generated SIRT5-overexpressing transgenic (SIRT5 Tg) mice in which expression of mouse SIRT5 fused with FLAG tag at the C-terminus was driven by the CAG promoter (Fig. 2A). Southern blot analysis was performed for genotyping (Fig. 2B), and two independent SIRT5 Tg mouse lines were established on the C57BL/6 inbred background (Fig. 2C). One of these, mouse line #36, was generated with a low copy number of transgene; the other, mouse line #38, was generated with a high copy number of transgene. SIRT5 Tg mice showed no gross anatomical or reproductive defects. In addition, no histological abnormality was observed by light microscopic analysis in all of the organs examined. To investigate the expression of SIRT5 protein, an antibody specific for mouse SIRT5 was raised in a rabbit against a synthetic peptide corresponding to 15 C-terminal amino acid residues (CGKTLPEALAPHETE) of mouse SIRT5, which shows no similarity to other members of the SIRT family. To ascertain specificity of the antibody, mitochondrial proteins were prepared from COS7 cells transfected with the expression plasmid encoding mouse SIRT5 protein fused with FLAG tag,

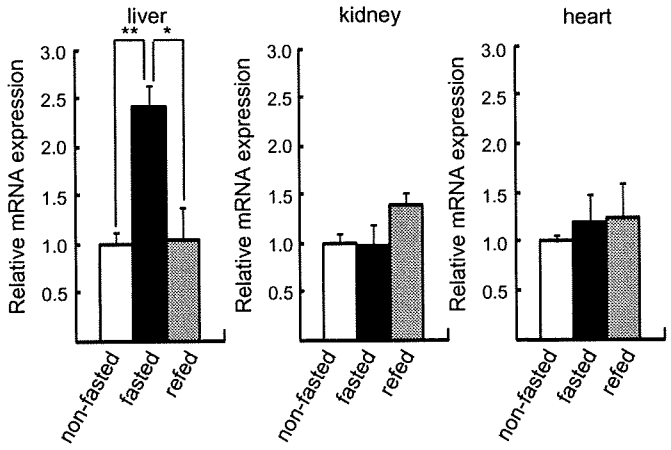

Fig. 1. Alteration of expression levels of SIRT5 mRNA by fasting and refeeding. Total RNA was isolated from livers, kidneys and hearts of 11 week-old C57BL/6 mice. Mice were divided into three groups: non-fasted ($N = 4$, open bars), fasted ($N = 4$, filled bars), and refed ($N = 4$, gray bar). The non-fasted group was fed *ad libitum*, the fasted group was fasted for 24 h, and the refed group was fasted for 24 h followed by normal chow for 24 h. The expression levels of SIRT5 mRNA were estimated by quantitative RT-PCR. SIRT5 mRNA levels were corrected for β-actin mRNA levels. Values are means ± SEM. $^{*}P < 0.05$. $^{**}P < 0.01$.

and western blotting was performed using the obtained anti-SIRT5 antibody or anti-FLAG antibody. A single band at ~32 kDa corresponding to the molecular weight of SIRT5–FLAG protein was detected with each antibody (Fig. 2D), demonstrating that this antibody specifically recognizes SIRT5 protein. Western blot analysis of mitochondrial proteins prepared from livers of the two SIRT5 Tg mouse lines using the anti-SIRT5 antibody showed that both endogenous 32-kDa SIRT5 protein and a SIRT5–FLAG protein with a molecular size somewhat larger were present, and that expression of SIRT5–FLAG protein was more abundant than that of endogenous SIRT5 protein in both Tg mouse lines (Fig. 2E).

Identification of CPS1 as a target of SIRT5 protein

Since SIRT5 mRNA levels were significantly upregulated in liver by fasting, we attempted to identify the protein that is modified by SIRT5 protein in liver. We hypothesized that deacetylation of the SIRT5 target protein might be facilitated by overexpression of SIRT5 in SIRT5 Tg mice. Because NAD-dependent deacetylase converts acetylated lysine to lysine of the target protein, its isoelectric point should shift to a higher pH value. Therefore, we performed two-dimensional electrophoresis to compare mitochondrial proteins prepared from livers of SIRT5 Tg mice and wild-type littermates; the protein samples were applied for isoelectric focusing electrophoresis, and separated by SDS-PAGE followed by staining with SYPRO Ruby. One of the proteins that newly appeared in SIRT5 Tg liver (Fig. 3A, indicated by arrow) was isolated, treated with trypsin, and analyzed by MALDI-TOF-MS (Fig. 3B). The sequences identified by mass spectrometry covered the N-terminal segment of carbamoyl phosphate synthetase 1 (CPS1) (Table. 1), suggesting that the protein is CPS1. CPS1 is a mitochondrial protein

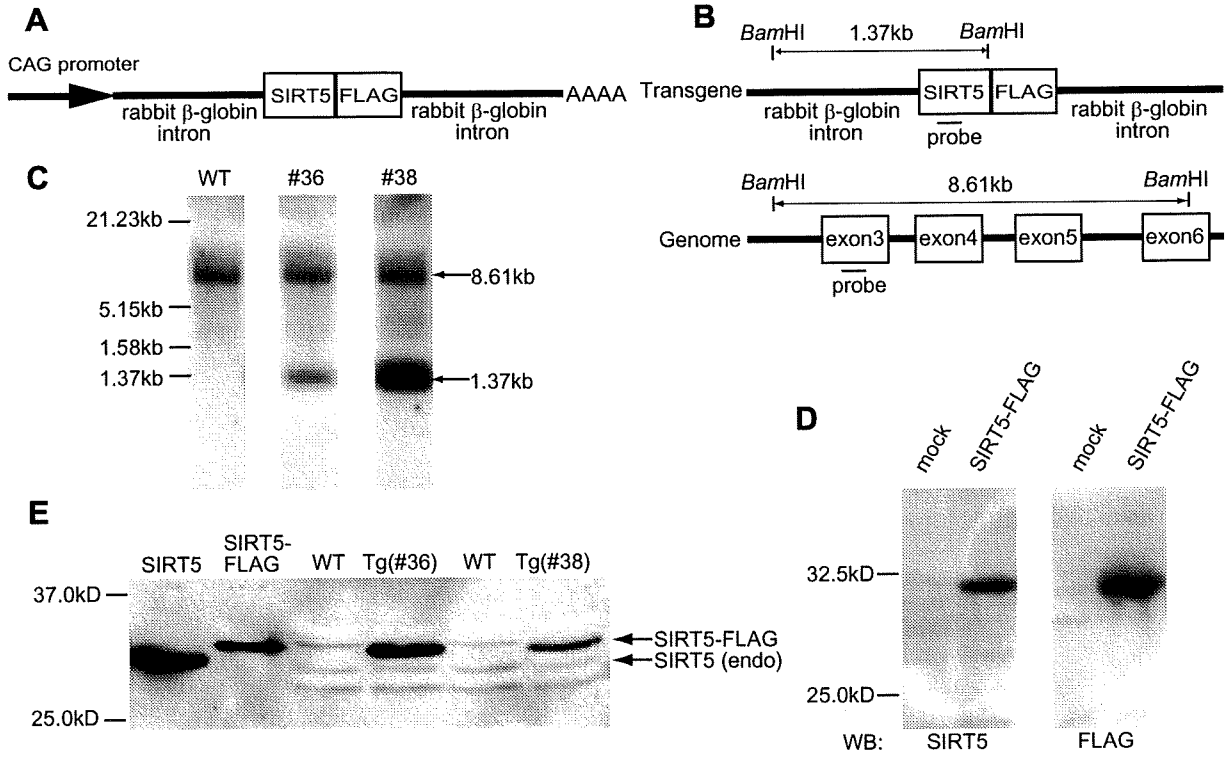

Fig. 2. Generation of SIRT5-overexpressing transgenic (SIRT5 Tg) mice and anti-SIRT5 antibody. (A) Scheme of the transgene used to generate SIRT5 Tg mice. The CAG promoter drives expression of mouse SIRT5 fused with FLAG tag at the C-terminus (SIRT5–FLAG). (B) Location of probes for Southern blot analysis. The probe corresponding to the DNA sequence in exon3 of mouse SIRT5 gene detects an 8.61-kb fragment in genomic DNA and a 1.37-kb fragment in the transgene after digestion with *Bam*HI. (C) Southern blot analysis of *Bam*HI-digested genomic DNA of wild-type (left panel) and SIRT5 Tg mice (middle panel: #36 transgenic mouse line, right panel: #38 transgenic mouse line). Southern blotting was performed with the probe indicated in (B). (D) Ascertainment of anti-SIRT5 antibody. The plasmid encoding mouse SIRT5 protein fused with FLAG tag (pCMV5aSIRT5–FLAG) was transfected to COS7 cells. Mitochondrial proteins were prepared from transfected and mock-transfected cells, and western blotting was performed with anti-SIRT5 antibody (left panel) and anti-FLAG antibody (right panel). (E) Overexpression of SIRT5–FLAG protein in SIRT5 Tg mice. Mitochondrial proteins were prepared from cells transfected with the plasmid encoding mouse SIRT5 without (pCMV5aSIRT5) or with FLAG (pCMV5aSIRT5–FLAG) and from livers of SIRT5 Tg mice and wild-type littermates (#36 and #38 transgenic mouse lines), and western blot analysis was performed using anti-SIRT5 antibody. Endogenous SIRT5 (endo) and SIRT5–FLAG proteins are indicated by arrows.

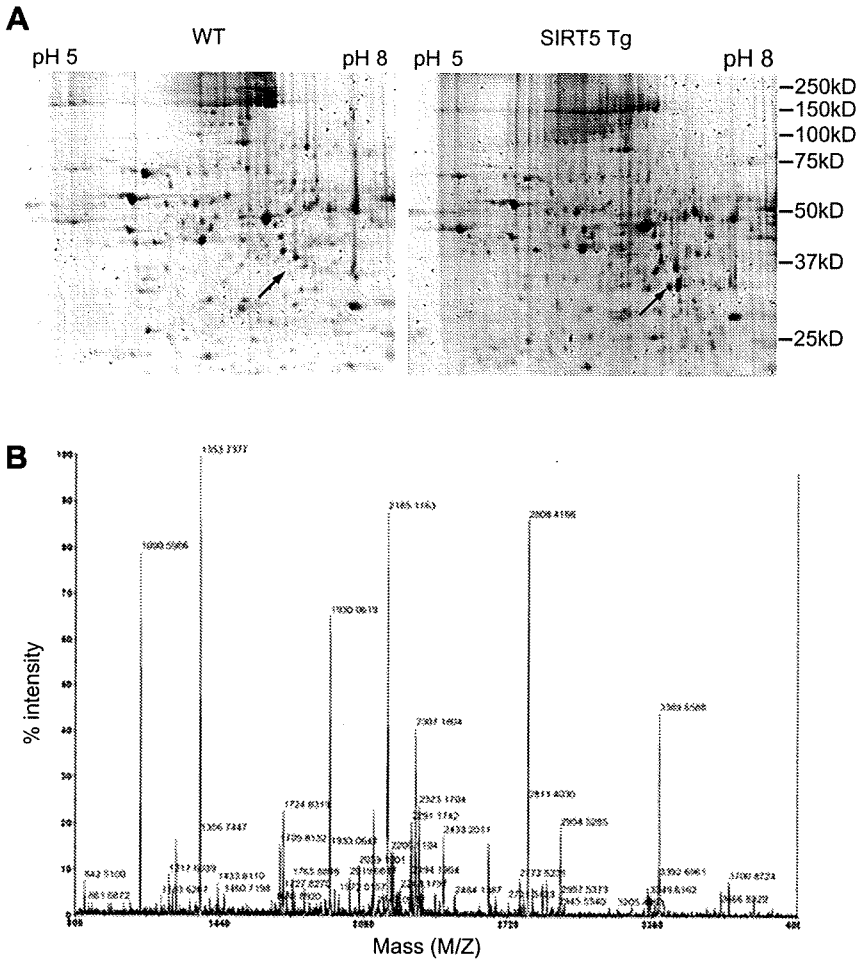

Fig. 3. Identification of the target protein of SIRT5. (A) Two-dimensional electrophoresis of mitochondrial proteins prepared from livers of SIRT5 Tg and wild-type mice. The position of the mitochondrial protein prepared from SIRT5 Tg liver identified by MALDI-TOF-MS is shown by arrow (right panel). The protein is not detected at the corresponding position (indicated by arrow, left panel) in wild-type liver. (B) MALDI-TOF-MS analysis. The mitochondrial protein prepared from SIRT5 Tg liver indicated in (A) was analyzed using MALDI-TOF-MS.

Table 1
Characterization by MALDI-TOF-MS of the target protein of SIRT5.

Measured peptide mass (Da)	Predicted peptide sequence	Start–end
1090.5986	KVPAIYGVDTRM	157–166
1217.6039	KSLGQWLQEEKV	147–156
1353.7377	RGQNQPVLNITNRQ	316–327
1723.8272	KIEFEGQSVDFVDPNKQ	182–196
1930.0619	KEPLFGISTGNIITGLAAGAKS	287–306
2058.1598	RKEPLFGISTGNIITGLAAGAKS	286–306
2184.1154	KGQILTMANPIIGNGGAPDTTARD	90–111
2807.4071	KIEFEGQSVDFVDPNKQNLIAEVSTKD	182–206
2953.5338	KGQILTMANPIIGNGGAPDTTARDELGLNKY	90–118
3662.8010	KMKGYSFGHPSSVAGEVVFNTGLGGYPEALTDPAYKG	55–89

Mass of peptides corresponding to a tryptic digest of CPS1. The corresponding sequence and position (number of amino acid residues) in the sequence are indicated.

expressed predominantly in liver, and catalyzes condensation of ammonia and bicarbonate to carbamoyl phosphate, which is the first step in the urea cycle in liver [15,16].

CPS1 is deacetylated in SIRT5 Tg liver

Since CPS1 is known to be an acetylated protein [26], we investigated deacetylation of CPS1 protein by SIRT5. The mitochondrial protein prepared from livers of SIRT5 Tg and wild-type mice fed *ad libitum* were immunoprecipitated with an anti-acetylated lysine antibody followed by immunoblotting using anti-CPS1 antibody. Acetylated CPS1 protein levels in SIRT5 Tg ($N = 3$) mice were 40% lower than those in wild-type mice ($N = 3$), although total CPS1 expression levels were similar (Fig. 4A). To determine whether SIRT5 protein regulates CPS1 activities, livers of SIRT5 Tg and wild-type mice were homogenized and CPS1 activities were measured. CPS1 activities were significantly increased approximately 2-fold in SIRT5 Tg mice ($N = 5$, $P < 0.01$) compared to those in wild-type mice (Fig. 4B). These results demonstrate that SIRT5 protein deacetylates CPS1 and upregulates its activity in liver.

Urea production is upregulated in SIRT5 Tg hepatocytes

To verify that SIRT5 is involved in the urea cycle by regulating CPS1 activity, production of urea in primary cultured hepatocytes was evaluated. Primary hepatocytes were isolated from SIRT5 Tg and wild-type mice and incubated with ammonia, bicarbonate, and ornithine for 1 h, and the amount of urea synthesized was determined by measuring the urea concentration in the media. Hepatocytes from SIRT5 Tg mice produced more urea than those of wild-type mice (44%, $N = 4$, $P < 0.01$) (Fig. 4C), indicating that urea synthesis is upregulated by overexpression of SIRT5 in liver.